# Stratigraphy, Geochronology, Paleoenvironments, and Depositional Controls of the Lower–Middle Santa Fe Group along the Ceja del Rio Puerco, Northwestern Albuquerque Basin, New Mexico

Daniel J. Koning[1], Julia Ricci[1], Matthew T. Heizler[1], Sean D. Connell[1], Jeremy K.C. Rugenstein[2], and Gary S. Morgan[3]

[1] New Mexico Bureau of Geology and Mineral Resources, New Mexico Institute of Mining and Technology, 801 Leroy Place, Socorro, NM 87801; dan.koning@nmt.edu

[2] Department of Geosciences, Colorado State University, 1482 Campus Delivery, Fort Collins, CO 80523

[3] New Mexico Museum of Natural History & Science, 1801 Mountain Road NW, Albuquerque, NM 87104

## Abstract

This paper documents a 400- to 600-m-thick succession of Miocene strata of the Santa Fe Group exposed along the Ceja del Rio Puerco, approximately 16–20 km west of Rio Rancho, New Mexico, United States. Eight new $^{40}Ar/^{39}Ar$ ages from tephra and detrital sanidine grains in sandstones are integrated with previously published biostratigraphic and magnetostratigraphic data to refine depositional ages and paleoenvironmental interpretations. Stratal accumulation rates (not corrected for compaction) and tilt-rate estimates indicate syntectonic deposition throughout the interval of interest, with a reduction in tilt rates after 14–13 Ma and a decrease in stratal accumulation rates after 14 Ma.

The succession includes the sandstone-dominated Zia and Cerro Conejo Formations (21–9 Ma), which are overlain by the gravel-bearing, upper Miocene Arroyo Ojito Formation (10–7 Ma). The Zia Formation records a transition from dominantly eolian deposition in the Piedra Parada Member (21–19 Ma) to sandy fluvial and subordinate eolian sedimentation at the piedmont–basin floor interface in the Chamisa Mesa Member (19.0–18.1 Ma). This shift likely reflects reorganization of a fluvial system that served as a sand source to the earlier eolian deposit. The overlying Cañada Pilares Member of the Zia Formation (18.1–17.5 Ma) consists of clay-rich deposits interpreted to be a playa-lake or floodplain depositional environment. We retain the original upper contact of the Cañada Pilares Member at the top of a 30- to 38-m-thick, reddish-brown, clay-rich interval.

A cryptic intraformational unconformity within 30 m above the base of the Cerro Conejo Formation separates 17.5–17.0 Ma strata from overlying 15–9 Ma strata. Three stratigraphic units are recognized within the Cerro Conejo Formation: (1) a western-piedmont unit, (2) a northern-fluvial unit deposited by a southward-flowing fluvial system that constructed a broad fan extending eastward beyond present-day Rio Rancho, and (3) an interfingering and mixed unit that includes the western-piedmont unit and a slightly finer-grained version of the southward-flowing fluvial system along the eastern margin of the western piedmont.

The sand-dominated Cerro Conejo Formation is overlain by and partly interfingers with the conglomeratic Arroyo Ojito Formation. The western part of the Arroyo Ojito Formation (in the study area) consists of the pale-brownish Navajo Draw Member to the east that interfingers westward with the Benavidez Member. We formally propose the Benavidez Member of the Arroyo Ojito Formation and present a type section that illustrates the lithologic character of this unit: reddish-yellow to tan, sandstone-dominated, tabular-bedded deposits containing ≥1% gravel. The Benavidez Member is the gravelly, more proximal extension of western-piedmont deposition during the late Miocene.

We infer tectonic, paleoclimatic, and substrate controls on deposition. Tectonic subsidence along the Moquino fault near the eastern margin of the Colorado Plateau is interpreted to have localized clay-rich deposition between 18.1 and 17.5 Ma (Cañada Pilares Member) and again at 14.1–14.0 Ma (green marker bed in the Cerro Conejo Formation). Between 13 and 10 Ma, the western piedmont prograded more than 4 km basinward (eastward). This progradation may reflect (1) a shift toward a paleoclimate with a greater proportion of summer precipitation and possibly more intense runoff events, and/or (2) increased displacement rates on major normal faults east of the Ceja del Rio Puerco (e.g., San Ysidro and Zia faults). Faulting to the east would effectively narrow the basin, focus aggradation on the hanging walls of the eastern faults, and promote a bypass surface and lower stratal accumulation rates in the study area west of these faults. An increase in gravel content within the Arroyo Ojito Formation at 10 Ma may reflect channelization over much of the medial-proximal piedmont, which would have promoted gravel transport to the distal piedmont and adjoining basin floor. Conversely, the increased volume of gravels could reflect progressive denudation in headwater regions that exposed Upper Cretaceous strata; their relatively low permeability may have sufficiently enhanced runoff and discharge capacity to transport gravel. Either process could have been promoted by (1) emergence after ~10 Ma of the Sierra Nacimiento as a paleotopographic feature that focused paleoflow into fewer paleorivers with relatively higher discharges (evidence for this paleohighland is based on the provenance of gravel in the post-10 Ma Arroyo Ojito Formation), and/or (2) possible uplift along the Jemez lineament.

## Introduction

This study focuses on the stratigraphy and sedimentary features of the Santa Fe Group in the Ceja del Rio Puerco, a region characterized by steep slopes and badland topography, about 16–20 km west of Rio Rancho and 30 km northwest of Albuquerque in north-central New Mexico, United States (Fig. 1). Located between the western edge of the Llano del Albuquerque and the eastern floor of the Rio Puerco valley, these steep slopes erode readily and provide excellent exposures of sandstone-dominated strata of the Santa Fe Group. The Santa Fe Group is a formal term applied to the syntectonic, clastic-dominated sedimentary deposits and minor intercalated volcanic flows that fill basins of the Rio Grande rift (Spiegel and Baldwin, 1963).

The study area lies in the western part of the Calabacillas subbasin (Fig. 1) of the larger Albuquerque Basin (Connell, 2004; Grauch and Connell, 2013). The Calabacillas subbasin is generally asymmetric, with basin fill thickening to the east. Only about 1 km of Santa Fe Group strata is exposed in the Ceja del Rio Puerco, whereas these strata are 3–5 km thick in the eastern basin (Connell, 2008a; Grauch and Connell, 2013). East-down displacement along faults in the western basin (e.g., San Ysidro and Sand Hill faults), combined with a condensed stratigraphic section, explains this thickness discrepancy. Most of the strata exposed on the Ceja del Rio Puerco can be correlated eastward into the subsurface using data derived from deep water-supply wells (Connell, 2008a; Koning et al., 2026a, 2026b). Therefore, detailed studies of the Ceja del Rio Puerco (and similar well-exposed escarpments and badlands north of La Ceja to the northeast of Ceja del Rio Puerco; Fig. 1) are useful for understanding the stratigraphic architecture of the Santa Fe Group in the Calabacillas subbasin. The fact that the Santa Fe Group provides nearly all of the groundwater supply for the City of Rio Rancho (Koning et al., 2026a, 2026b) underscores the hydrogeologic importance of such work.

The main purposes of this study are to systematically describe lithostratigraphic units of the 400- to 600-m-thick lower–middle Santa Fe Group exposed on and below the Ceja del Rio Puerco, integrate new and preexisting age control from vertebrate fossils and $^{40}Ar/^{39}Ar$ data, discuss stratigraphic relations between units, and provide updated interpretations of depositional environments. Our study highlights the internal stratigraphy of the Cerro Conejo Formation and establishes a type section for the proposed Benavidez Member of the Arroyo Ojito Formation. We also discuss possible paleoclimatic and tectonic controls on the stratigraphic succession. Most of this material is synthesized from 1:24,000-scale geologic mapping (Koning and Jochems, 2014; Koning and Rawling, 2017). Additional data are provided by a lithostratigraphic study conducted in conjunction with recent paleoclimate research using stable isotope analyses of authigenic carbonates (Rugenstein et al., 2026).

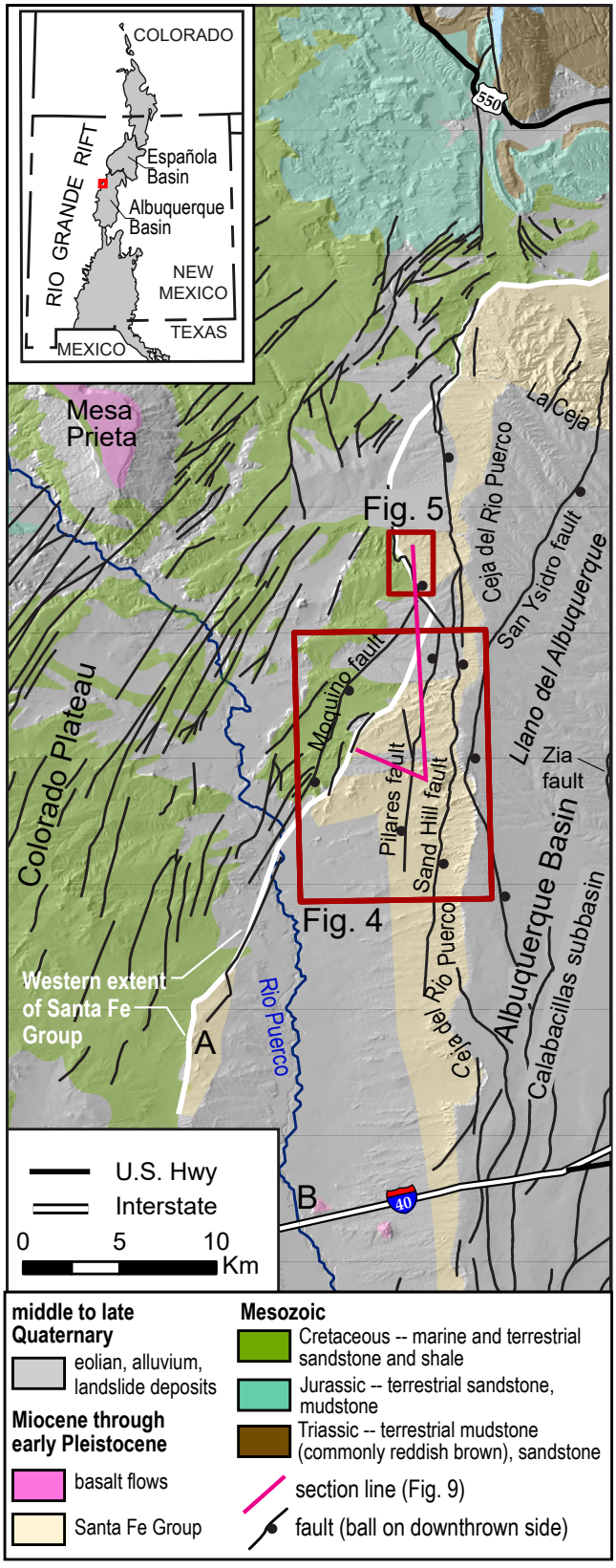



Figure 1. Location of study area relative to the Rio Puerco valley, Ceja del Rio Puerco, and Llano del Albuquerque. Position of study within the larger Rio Grande rift and New Mexico is shown in the inset map (top left). Within the extent of this figure, the study area corresponds to two red rectangles (i.e., the two geologic maps of Figs. 4 and 5). "A" shows outcrops where pebble-bearing sandstones in the middle Piedra Parada Member (Zia Formation) are found (Koning and Jochems, 2014; Rawling and Koning, 2019). "B" denotes the northwest side of La Mesita Negra, where the Benavidez Member underlies an 8.1 Ma basalt flow (Maldonado et al., 2006). The bright pink line corresponds to the stratigraphic correlation diagram of Figure 9.

### *Previous Work*

The exposures along the Ceja del Rio Puerco have captured the attention of geologists for nearly a century, especially since most of the Santa Fe Group in the Albuquerque Basin is poorly exposed. The earliest investigations of the Santa Fe Group recognized three informal stratigraphic units: the lower gray, middle red, and upper buff members within the Santa Fe Formation (Fig. 2; Bryan and McCann, 1937, 1938; Wright, 1946; Spiegel, 1961). Note that the Santa Fe stratigraphic unit was originally defined at formation rank but was later raised to group rank by Spiegel and Baldwin (1963); however, this change was not universally accepted until the 1980s. The lower gray unit was renamed the Zia Sand Formation (Galusha, 1966) and was subdivided into three members (listed here in ascending order): Piedra Parada, Chamisa Mesa, and Cañada Pilares (Galusha, 1966; Gawne, 1981a). The stratigraphic nomenclature of Kelley (1977) proposed formalizing two members within the Santa Fe Formation: the Ceja Member (formerly the upper buff member) and the Zia Member (downgrading the Zia Formation of Galusha [1966] to member status). Later publications (Tedford and Barghoorn, 1997, 1999; Connell et al., 1999; Connell, 2004, 2008a, 2008b) established the stratigraphic usage widely employed today (listed here in ascending order): (1) Zia Formation (with the Piedra Parada, Chamisa Mesa, and Cañada Pilares Members), (2) Cerro Conejo Formation, (3) Arroyo Ojito Formation (with Navajo Draw, Loma Barbon, and Picuda Peak Members), and (4) Ceja Formation (Fig. 2). See Connell (2008b) for a diagram illustrating the evolution of stratigraphic nomenclature.

Other efforts that advanced understanding of the stratigraphy and sedimentology of the Santa Fe Group at the Ceja del Rio Puerco include fossil investigations, geologic mapping, and studies of cementation processes. Fossil investigations focused on the terrestrial vertebrate fauna and were led by Richard Tedford (Tedford, 1981, 1982; Tedford and Barghoorn, 1997, 1999) and later by Gary Morgan (Morgan and Williamson, 2000, 2007). Germane geologic mapping efforts include those of Cather et al.

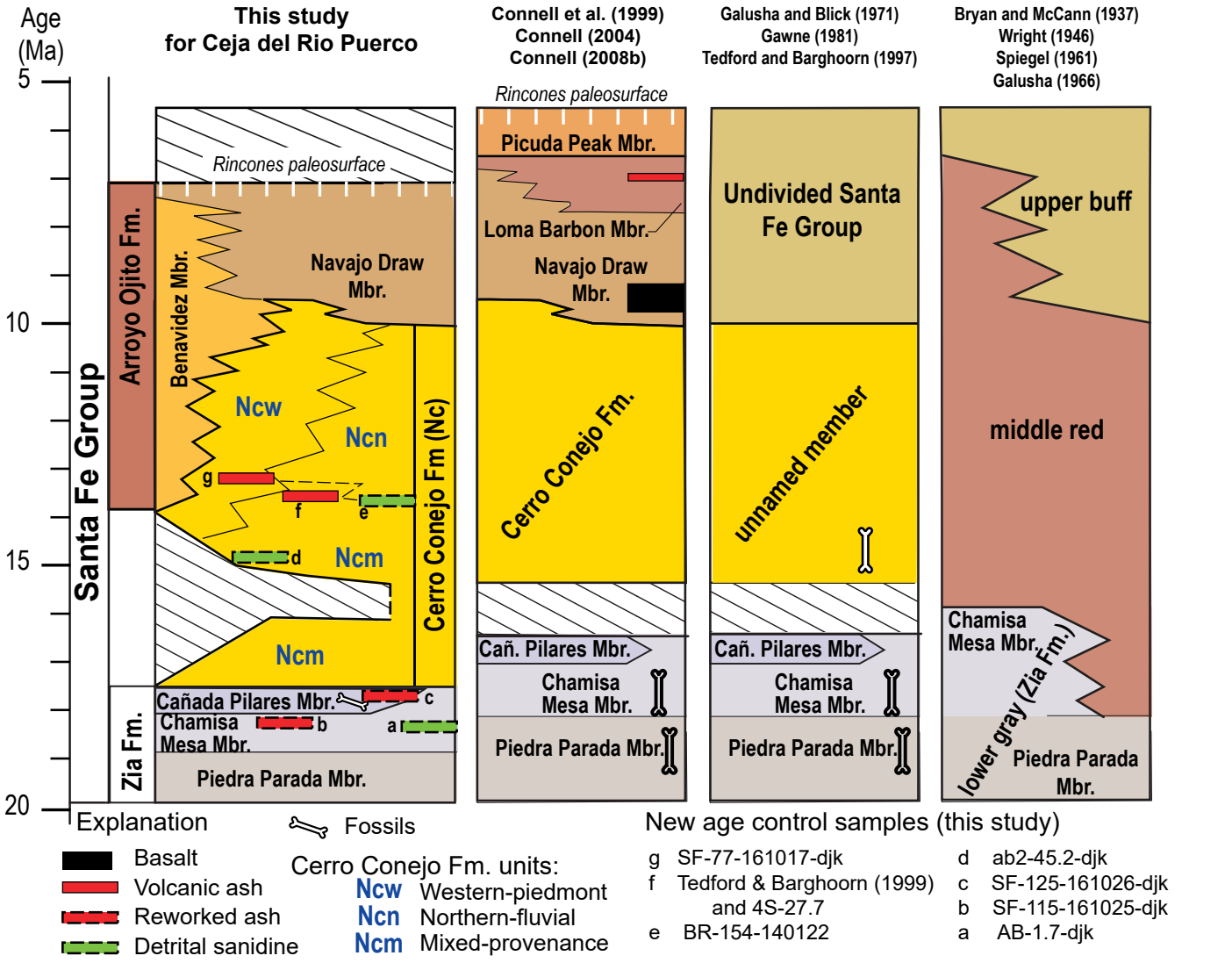



Figure 2. (Left panel) Stratigraphic relations and age control of the lower–middle Santa Fe Group in the Ceja del Rio Puerco study area. (Right panels) Stratigraphic schemes of previous workers (compiled from fig. 2 of Connell, 2008b) that apply to the larger northwestern Albuquerque Basin. In each column, basin-proximal elements are shown on the left side, and basin-center elements are shown on the right.

(1997), Koning et al. (1998), Williams and Cole (2007), Connell (2008a), Thompson et al. (2009), Cikoski et al. (2012), Koning and Jochems (2014), Koning and Rawling (2017), and Rawling and Koning (2019). Beckner and Mozley (1998) documented cementation processes in the sandstones of the Cerro Conejo and Zia Formations. Smyth (2004) and Brandes (2002) studied the sedimentology and petrology of the Arroyo Ojito Formation.

## Methods

### *Field*

Santa Fe Group strata were mapped and described using standard field procedures (e.g., Compton and Compton, 1985) and interpretation of aerial photographs (U.S. Department of Agriculture, 2009). Photogrammetric software ("Stereo Analyst for ArcGIS" Hexagon Geospatial) allowed direct digitization of contacts and other features into GIS using these aerial photographs and GPS waypoints. Stratigraphic sections were measured utilizing a Jacob staff, an Abney level, and a handheld GPS. Note that we did not measure the upper half of the Cerro Conejo Formation. Instead, for those strata, we used the stratigraphic section of Tedford and Barghoorn (1999).

### *Magnetostratigraphy*

We measured our stratigraphic sections within ~0.5 km (N–S) of those of Tedford and Barghoorn (1999) and projected their magnetostratigraphic data into our stratigraphic sections. Unfortunately, Tedford and Barghoorn (1999) did not describe their magnetostratigraphic procedures. Note that their samples were coarsely spaced (5–25 m vertical). This means correlations to the Global Polarity Time Scale (GPTS) are relatively tenuous away from samples with $^{40}Ar/^{39}Ar$ age control described below; this is particularly the case for samples in the upper half of the Cerro Conejo Formation.

### *$^{40}Ar/^{39}Ar$ Geochronology*

Volcanic ash (tuff), sandstone, and conglomerate samples were collected from eight field localities for $^{40}Ar/^{39}Ar$ geochronology (Fig. 3). During sampling, highly altered outcrops were avoided. Sanidine crystals were extracted from volcanic tuff-bed samples and detrital sanidines (DS) from sandstone samples using standard mineral separation procedures (samples listed in Table 1). Samples were first sieved and then treated with dilute hydrofluoric acid (HF) in an ultrasonic bath for 10–15 minutes to remove surface contamination, secondary clay phases, and carbonate grains. This treatment was followed by three rinses in deionized water. Sanidine grains were further concentrated by density separation over a narrow density interval and subsequently handpicked using wintergreen oil under a binocular microscope.

The volcanic gravel clast sample (Table 2; SF-50b-161017-djk) was prepared by crushing and treating with dilute hydrochloric acid (HCl) in an ultrasonic bath for 10–15 minutes to remove surface contamination, secondary clay phases, and carbonate material, followed by three rinses in deionized water. Hornblende grains free of visible inclusions were then handpicked under a binocular microscope.

To perform the $^{40}Ar/^{39}Ar$ analyses, samples were irradiated for 8 hours at the U.S. Geological Survey TRIGA reactor in Denver, Colorado. The Fish Canyon Tuff sanidine (FCS) standard, with an assigned age of 28.201 ± 0.023 Ma (Kuiper et al., 2008), was used as the neutron flux monitor. The J-value for each sample was determined using a combination of six single-grain laser fusion analyses measured at eight radial positions around the irradiation disc. Correction factors for interfering neutron reactions were determined using co-irradiated $CaF_2$ and K-glass. The total decay constant of $5.463 \times 10^{-10}$/yr (Min et al., 2000) and the $^{40}Ar/^{36}Ar$ atmospheric ratio at 295.5 ± 0.5 (Nier, 1950) were used for age calculations. Sanidine crystals were analyzed by total fusion using a $CO_2$ laser, and argon isotopes were measured with a ThermoFisher Scientific Argus VI multicollector

Table 1. Geochronologic data for tuff and sandstone samples in the lower–middle Santa Fe Group.

| | UTM Coordinates* | | | | | |
|---|---|---|---|---|---|---|
| **Sample** | **Easting (m)** | **Northing (m)** | **Material** | **Weighted Mean Age ± 2σ (Ma)** | **N/Total** | **MSWD** |
| **Cerro Conejo Formation** | | | | | | |
| SF-77-161017-djk | 327614 | 3913516 | Sanidine | 13.12 ± 0.10 | 3/4 | 0.6 |
| 4S-27.7 | 328669 | 3902766 | Sanidine | 23.03 ± 0.08 | 1/49 | na |
| BR-154-140122 | 325147 | 3901238 | Sanidine | 13.77 ± 0.32 | 1/7 | na |
| ab2-45.2-djk | 329728 | 3905625 | Detr sanidine | 14.87 ± 0.08 | 2/195 | 1.6 |
| **Cañada Pilares Member (Zia Formation)** | | | | | | |
| SF-125-161026-djk | 329502 | 3905838 | Sanidine | 18.36 ± 0.14 | 5/48 | 0.1 |
| **Chamisa Member (Zia Formation)** | | | | | | |
| SF-115-161025-djk | 329204 | 3905989 | Sanidine | 18.10 ± 0.46 | 3/47 | 1.6 |
| AB-1.7-djk | 329174 | 3905974 | Detr sanidine | 18.26 ± 0.06 | 1/196 | na |

Ages calculated relative to Fish Canyon Tuff sanidine with a value of 28.201 ± 0.023 Ma (Kuiper et al., 2008) and the total $^{40}K$ decay constant of Min et al. (2010). Detr = detrital; MSWD = mean square of weighted deviates; N = number of analyses.
* UTM coordinates are for zone 13 and in NAD83.

Table 2. Geochronologic data for volcanic gravel at base of Piedra Parada Member, Zia Formation.

| Sample | Material | Spectrum Age ± 2σ (Ma) | N/Total | MSWD | Integrated Age ± 2σ (Ma) | Isochron Age ± 2σ (Ma) | $^{40}Ar/^{36}Ar$ | N | MSWD |
|---|---|---|---|---|---|---|---|---|---|
| SF-50b-161017-djk* | Hornblende | **33.7 ± 1.1** | 8/8 | 1.5 | 33.9 ± 1.3 | 33.5 ± 1.4 | 296 ± 5 | 8/8 | 1.8 |

Age calculated relative to Fish Canyon Tuff sanidine with a value of 28.201 ± 0.023 Ma (Kuiper et al., 2008) and the total $^{40}K$ decay constant of Min et al. (2010).
Bold ages represent the preferred ages. MSWD = mean square of weighted deviates; N = number of analyses used on total analyses done.
* Sample location is 325,605 m E, 3,906,263 m N (UTM coordinates in zone 13, NAD83).

mass spectrometer. For tuff samples with small sanidine grains, multigrain analyses were also performed; 5–10 grains were ablated by the laser and measured collectively. Hornblende grains were analyzed using the incremental step-heating method with a defocused diode laser, and argon isotopes were measured with a ThermoFisher Scientific Helix MC multicollector mass spectrometer.

The maximum depositional ages for detrital sanidine samples and reworked tuffs were calculated as the inverse-variance-weighted mean of the youngest statistically coherent age population, evaluated using the mean square of weighted deviates (MSWD). For primary tuffs, eruption ages were calculated from the interpreted juvenile sanidine population. Data reduction and age calculations were performed using MassSpec software. All uncertainties are reported at the 2σ confidence level (Fig. 3).

## Results

Here we present results related to lithostratigraphy and new age control. We describe units of the Zia, Cerro Conejo, and lower Arroyo Ojito Formations from oldest to youngest (Fig. 2), using data primarily obtained during geologic mapping (Koning and Jochems, 2014; Koning and Rawling, 2017) and our stratigraphic sections. The geologic context and structural information of these units are shown in two geologic maps located in Figure 1: one for the Ceja del Rio Puerco west of Southern Boulevard (Fig. 4) and the other for Navajo Draw to the north (Fig. 5). Figure 6 depicts the Arroyo Benavidez-01 and Arroyo Benavidez-02 stratigraphic sections covering the middle Chamisa Mesa Member (Zia Formation) through the lower Cerro Conejo Formation. Figure 7 illustrates the Southern Boulevard stratigraphic section (middle to upper Cerro Conejo Formation). The locations of both sections are shown in Figure 4. Detailed descriptions for these and other stratigraphic sections are given in Appendix 1[1]. Note that the described strata are mostly weakly cemented and weakly to well consolidated. Although most samples are not well indurated, we use the terms "sandstone," "mudstone," and "claystone" for all studied strata for consistency.

### *Zia Formation*

The Zia Formation includes the lower strata of the Santa Fe Group. The paleontology and sedimentological features of this unit were mainly studied by Galusha (1966), Gawne (1981a, 1981b), Tedford (1982), and Tedford and Barghoorn (1997, 1999). These workers have subdivided the formation into the following members, listed from oldest to youngest: Piedra Parada, Chamisa Mesa, and Cañada Pilares. The contacts between the three members are conformable. Except where noted, Zia Formation sandstone is generally subangular to rounded (mostly subrounded) and well to moderately sorted, and has 10–25% lithic grains. Grains are composed of subequal quartz, feldspar, and volcanic-dominated lithic grains, where intermediate volcanic compositions are more common than felsic compositions (Gawne, 1981a, 1981b). Refer to Gawne (1981a, 1981b) for a more detailed descriptive counterpart to what is presented below for the Zia Formation. Note that due to the asymmetric nature of the Albuquerque Basin (deeper to the east; Grauch and Connell, 2013), the members of the Zia Formation likely increase in thickness east of the Ceja del Rio Puerco.

#### Piedra Parada Member

##### *Lithostratigraphy*

The Piedra Parada Member is ~80–100 m thick and consists of white to light-gray (locally tan), medium-grained sandstone with local cross-stratification (Figs. 8A and 8B). Where present, tabular beds are medium to very thick and exhibit horizontal-planar laminations or cross-stratification (with foresets up to 3 m thick, although Gawne [1981b] noted foresets >4.5 m thick). The sandstone is medium- to coarse-grained (predominantly medium-grained, locally fine-grained), subrounded to rounded, and well sorted, and contains 15–30% lithic grains that are dominated by volcanic (felsic to intermediate) grains. On a millimeter scale, laminations can be bimodal, with grain size alternating between 0.15–0.5 mm and 0.35–1.0 mm. Locally, lenticular to broadly lenticular laminations are present and are interpreted to represent lobate grain flows (Bristow and Mountney, 2013). Tabular, bioturbated zones are present and commonly correspond to cemented beds, typically tens of centimeters thick, and are characterized by extensive burrowing. About 10 km southwest of the southwestern corner of the main study area (labeled A in Fig. 1), local chert and lesser rhyolite pebbles are present in the middle of the unit (Koning and Jochems, 2014; Rawling and Koning, 2019). The Piedra Parada Member exhibits outcrops with ~5–35% strong cementation by calcium carbonate. There are very minor, relatively thin, pinkish to orange, muddy sandstones and greenish calcareous mudstones (Gawne, 1981a, 1981b; Tedford and Barghoorn, 1999).

[1] Appendices are available for download at https://geoinfo.nmt.edu/repository/index.cfml?rid=20260001.

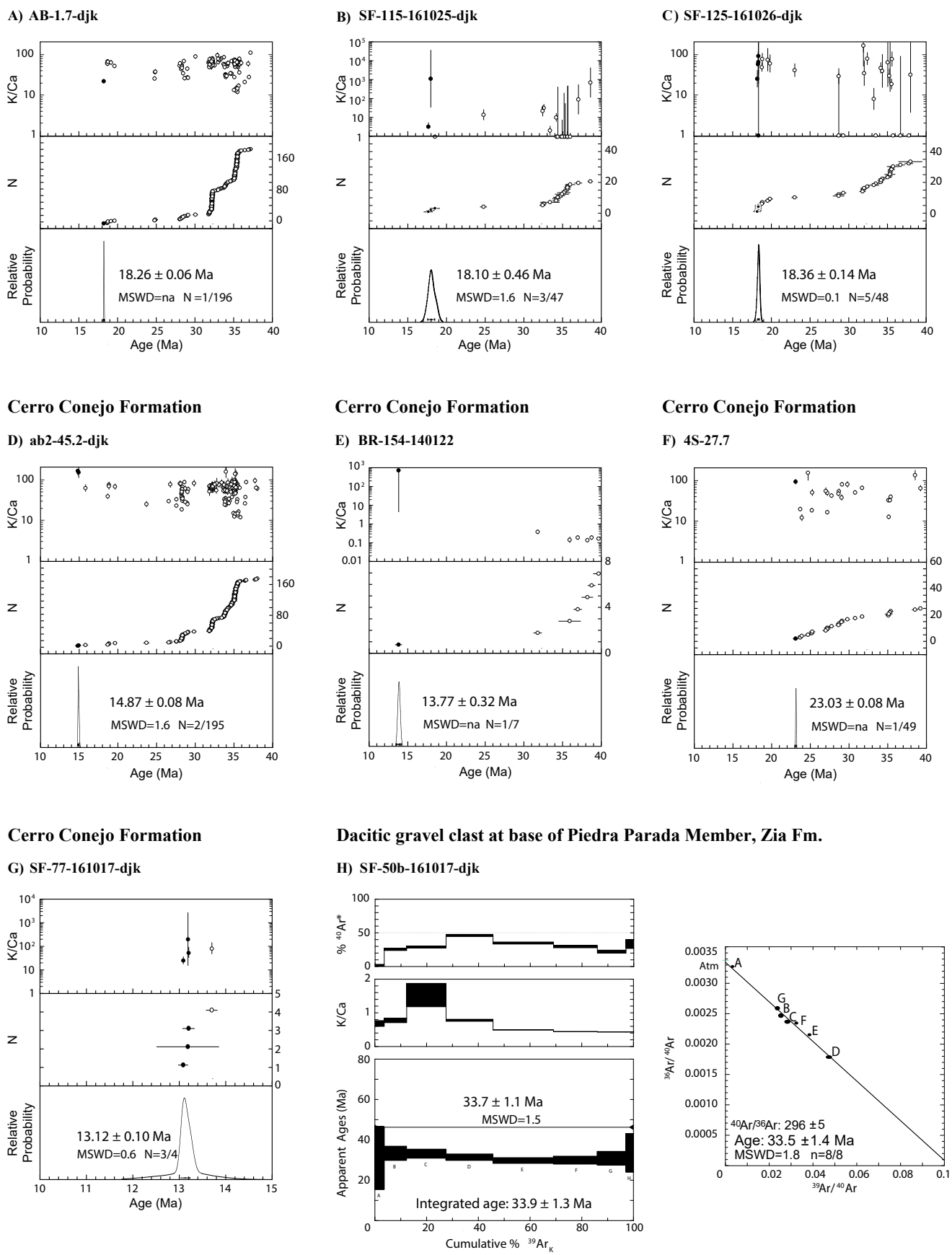



Figure 3. Plots of $^{40}Ar/^{39}Ar$ spectra for the volcanic tuff and detrital sanidine samples of (A) AB-1.7-djk, (B) SF-115-161025-djk, (C) SF-125-161026-djk, (D) ab2-45.2-djk, (E) BR-154-140122, (F) 4S-27.7, and (G) SF-77-161017-djk. Data for a volcanic gravel clast are in (H) SF-50b-161017-djk.

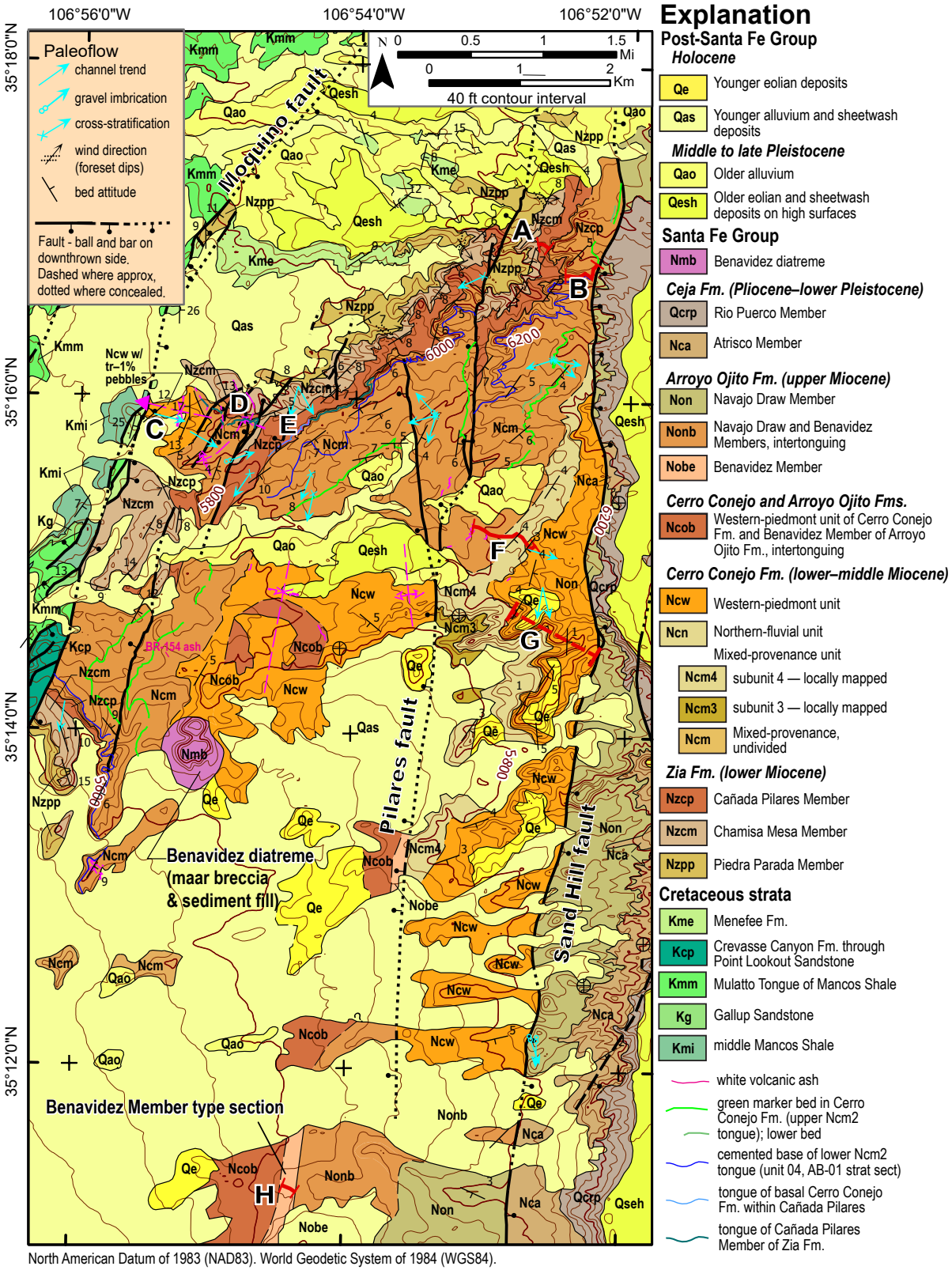



Figure 4. Geologic map of the main study area along Ceja del Rio Puerco. Compiled from Koning and Jochems (2014) and Koning and Rawling (2017). Thick, red lines indicate stratigraphic sections. Thick black letters note key locales, listed from north to south: (A) Arroyo Benavidez-01 stratigraphic section; (B) Arroyo Benavidez-02 stratigraphic section; (C) transverse syncline on Moquino fault and the Alice King Bypass Road stratigraphic section (Appendix 1B); (D) thin, western tongue (6–8 m thick) of Cañada Pilares Member within basal Cerro Conejo Formation strata; (E) intertonguing of upper Cañada Pilares Member (Zia Formation) and basal Cerro Conejo Formation strata; (F) Southern Boulevard stratigraphic section; (G) dashed, thick red line denotes upper part of Southern Boulevard stratigraphic section (>88 m) from Tedford and Barghoorn (1999); (H) type section for the Benavidez Member (Arroyo Ojito Formation).

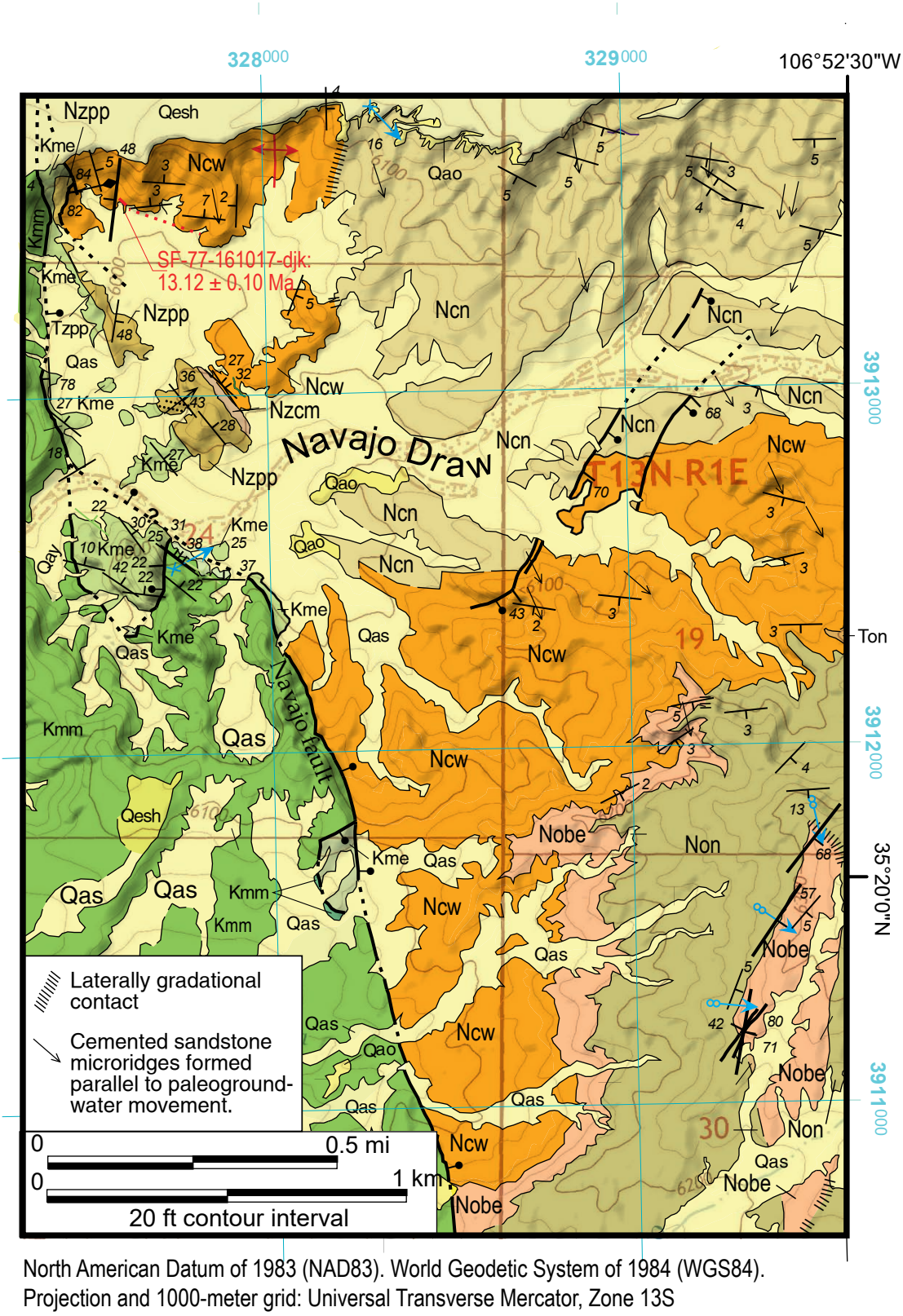



Figure 5. Geologic map of upper Navajo Draw drainage. Modified from Koning and Rawling (2017). Black arrow denotes inferred paleogroundwater flow direction. See Figure 4 for complete explanation of symbols and unit shading.

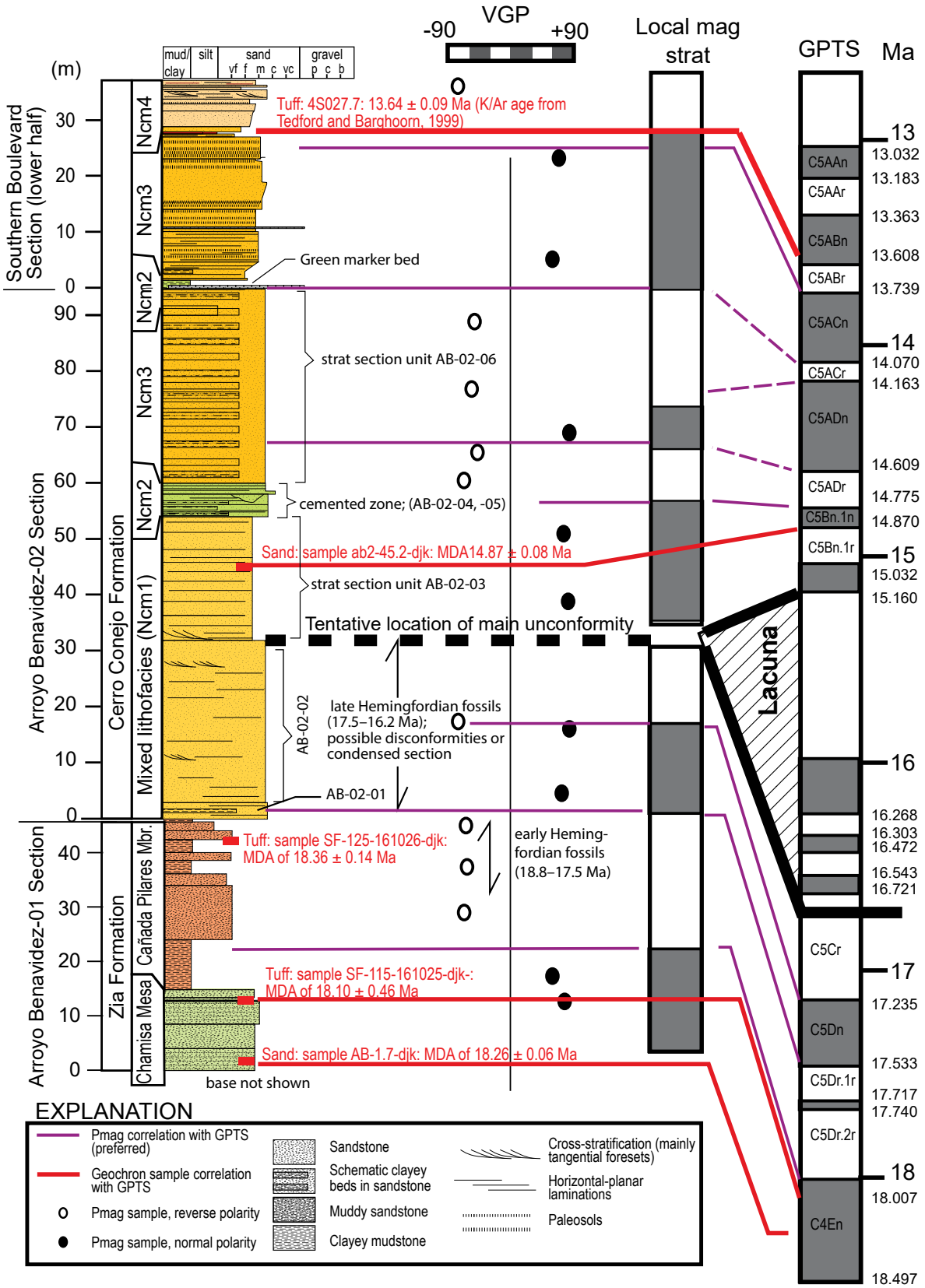



Figure 6. Graphic column of the Arroyo Benavidez stratigraphic section (on left), and correlation to Global Polarity Time Scale (GPTS, on right; Ogg, 2020). Measured and described by Jeremy Rugenstein, Daniel Koning, and Thu Bui. The unconformity, which is poorly constrained in the basal Cerro Conejo Formation, lies below sample ab2-45.2 and above the base of the Cerro Conejo Formation. This unconformity may be a single surface roughly 30 m above the base of the Cerro Conejo Formation (bolded dashed line labeled as "tentative location of main unconformity"), near the top of a stratigraphic interval bearing rare, late Hemingfordian (17.5–16.2 Ma) fossils (per Tedford and Barghoorn, 1997, 1999). However, in the 30-m interval, a series of disconformities and/or a condensed section may be present.

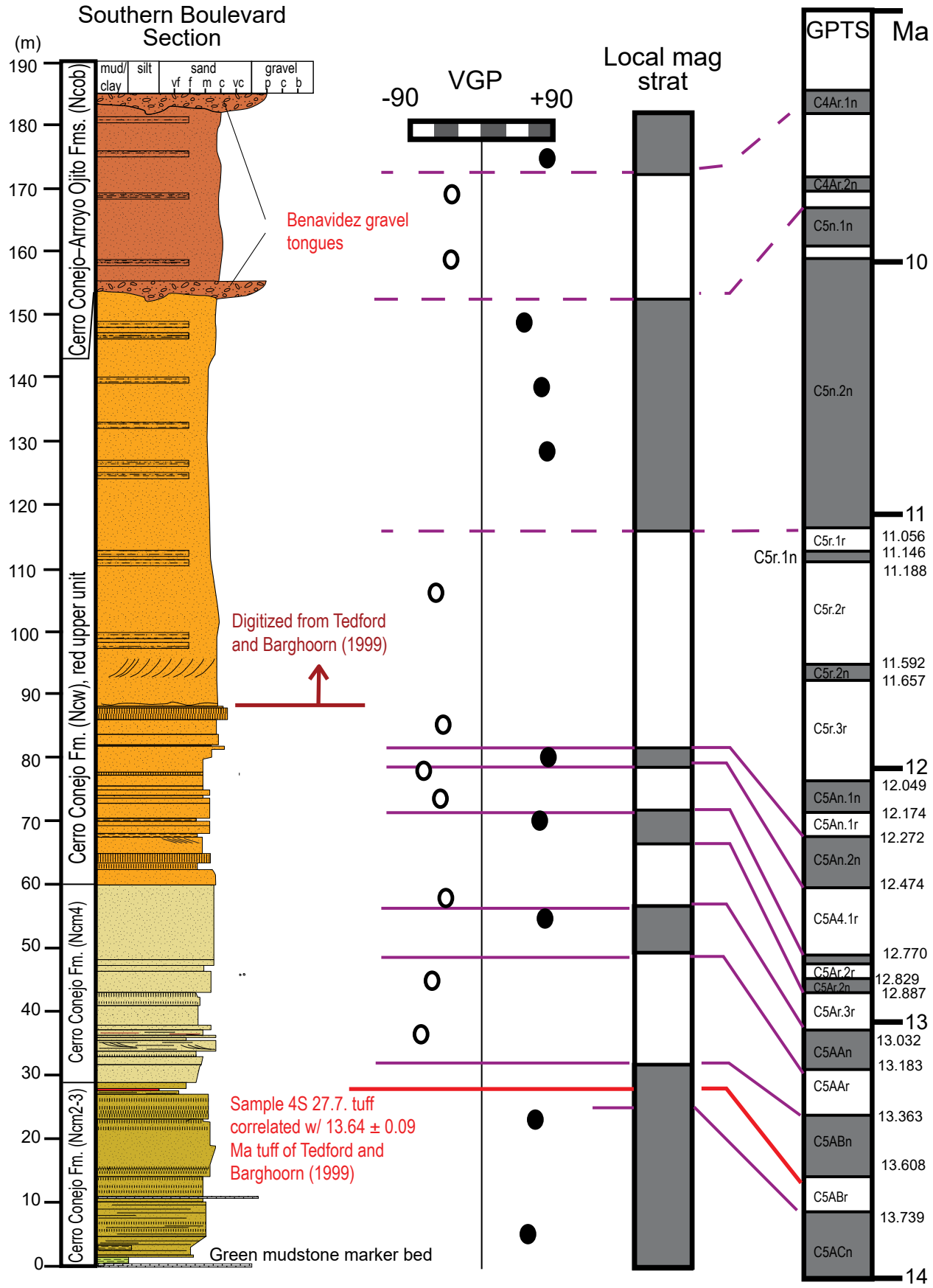



Figure 7. Southern Boulevard stratigraphic section and correlation to the Global Polarity Time scale (GPTS, on right; Ogg, 2020). Described and measured by Daniel Koning and Jeremy Rugenstein from 0 to 88 m. The upper part of the section is from Tedford and Barghoorn (1999) and shown as the dashed, thick red line in Figure 4. Explanation of symbols is given in Figure 6.

The lower and upper contacts of the Piedra Parada Member are informative. The basal contact corresponds to an unconformity that overlies paleotopographic relief developed on the underlying Menefee Formation. At the base of the unit commonly lie subrounded to rounded pebbles (~1 m thick) composed of chert, quartz, and quartzite, together with 1–30% light-gray, hornblende-biotite dacite clasts that locally exhibit ventifacting (Gawne, 1981b; Tedford and Barghoorn, 1999; Koning and Rawling, 2017). The upper contact grades upward and intertongues with the overlying Chamisa Mesa Member.

### *Geochronology*

The age of one of the basal dacite clasts (sample SF-50b-161017-djk) provides a maximum depositional age. The age spectrum defines a plateau age of 33.7 ± 1.1 Ma, characterized by at least three contiguous steps overlapping within 2σ uncertainty and at least 50% of the $^{39}$Ar released (Table 2, Fig. 3H; McDougall and Harrison, 1999). This plateau age has an associated MSWD value of 1.5, indicating a normal distribution at the 95% confidence level (Table 2; Mahon, 1996). No evidence of excess $^{40}$Ar or mass fractionation was detected, as evidenced by the $^{40}$Ar/$^{36}$Ar intercept values for the trapped argon aligning with the current atmospheric ratio of 295.5 ± 0.5 (Table 2, Fig. 3H; Nier, 1950).

## Chamisa Mesa Member

### *Lithostratigraphy*

The Chamisa Mesa Member overlies a gradational and intertonguing contact with the underlying Piedra Parada Member. This member is tentatively correlated to a 12-m-thick interval overlying Piedra Parada strata in Navajo Draw (Figs. 5 and 9). To the south, in the main study area, this member thickens to 30–35 m, according to mapping by Koning and Jochems (2014) and Koning and Rawling (2017), but Gawne (1981a, 1981b) gave a thickness of 16 m (encompassing the upper half of the Chamisa Mesa Member in the Koning maps). The Chamisa Mesa Member commonly contains medium to very thick, tabular beds (Fig. 8C) that exhibit laminations (horizontal-planar to cross-laminated in <30-cm-thick bed sets) or are structureless (massive). About 1–20% of strata are strongly cemented by calcium carbonate. Deposits consist of very fine- to medium-grained sandstone and silty, very fine- to fine-grained sandstone. Uncemented sand is pink to light brown to very pale brown. In most of the study area, there are sparse (up to 10%), reddish, medium to thick, and tabular beds of mixed claystone, siltstone, and very fine- to medium-grained sandstone, but these beds are not observed to the north near the drainage of Navajo Draw (Fig. 5). Bioturbation is relatively common and includes structureless beds, rhizoliths, and paleoburrows (Fig. 8D). In bioturbated beds, rhizoliths may occupy up to 5% of the exposure and are 0.5–2.0 cm wide. Paleoburrows are as much as 4 cm wide.

The Chamisa Mesa Member is lithologically similar to the Cerro Conejo Formation but differs markedly from the other two members of the Zia Formation. Compared to the lower Cerro Conejo Formation, the sandstone is slightly better sorted and slightly finer in the Chamisa Mesa Member, and cemented beds more commonly exhibit rhizoliths and paleoburrows. Compared to the Piedra Parada Member of the Zia Formation, the Chamisa Mesa Member exhibits more distinctive tabular-bedding, thick cross-bed sets are lacking, and the sandstone is slightly redder and finer. The Chamisa Mesa Member differs from the Cañada Pilares Member by having <10% clayey strata.

### *Geochronology*

Two new $^{40}$Ar/$^{39}$Ar ages were obtained. First, a detrital sanidine sample (AB-1.7-djk) collected 16 m below the upper contact returned a youngest-single-grain age of 18.26 ± 0.06 Ma, providing a maximum depositional age constraint (N = 1/196; Table 1, Figs. 3A and 6). Second, a 28-cm-thick tuff bed was sampled 2 m below the upper contact of the member and yielded an $^{40}$Ar/$^{39}$Ar age of 18.10 ± 0.46 Ma based on the three youngest statistically coherent populations out of the 47 analyzed grains (SF-115-161025-djk in Table 1; Figs. 3B and 6). Both single-grain and combined multigrain (~5–10 crystals) analyses were performed, and both displayed comparable age dispersion. The dispersed nature of sanidine ages of this tuff suggests fluvial reworking, and thus its interpreted age is a maximum depositional age (Table 1, Figs. 3A and 3B).

## Cañada Pilares Member

### *Lithostratigraphy*

The 28- to 38-m-thick Cañada Pilares Member of the Zia Formation is a slope-forming, reddish-brown, clay-rich mudstone interbedded with subordinate (locally subequal), 0.5- to 5-m-thick tongues of reddish sandstone and silty fine-grained sandstone (Figs. 8E–8H). Tedford and Barghoorn (1999) expanded the Cañada Pilares Member (as defined by Gawne [1981a, 1981b]) to include an overlying, ~30-m-thick sandstone interval with abundant cross-stratification. However, we follow the original definition of Gawne (1981a, 1981b), restricting this member to reddish-brown, claystone-rich strata lying between the sandstone-dominated Chamisa Mesa Member (Zia Formation) and the Cerro Conejo Formation (Fig. 8E). The lower contact of the Cañada Pilares Member is relatively sharp (≤15-cm-thick gradation). The upper contact is sharp or scoured to gradational, depending on locality, and locally intertongues with the overlying sandstones of the lower Cerro Conejo Formation, as noted by Tedford and Barghoorn (1999) (Figs. 8F and 8G; Fig. 4, site E). Note that this member is absent in and north of Navajo Draw, Ceja del Rio Puerco (Fig. 5). To the west, the Cañada Pilares Formation occurs as a 6- to 8-m-thick tongue within sandstones correlated to the Cerro Conejo Formation (Fig. 4, site D). The clayey mudstone exhibits very thin to medium, tabular beds. One or two sparse, thick beds of greenish mudstone occur near the top of the unit. These green mudstones are locally associated with tuffs and locally capped by thin limestone beds.

Sandstone tongues are up to ~6 m thick and exhibit very thin to thick, tabular beds (Fig. 8G; Koning et al., 2026c, fig. 2.28). Within these beds, the sandstone is structureless or vaguely horizontal-planar laminated. Locally, cross-stratification (foresets up to a few decimeters thick), ripple marks, and clay rip-up clasts

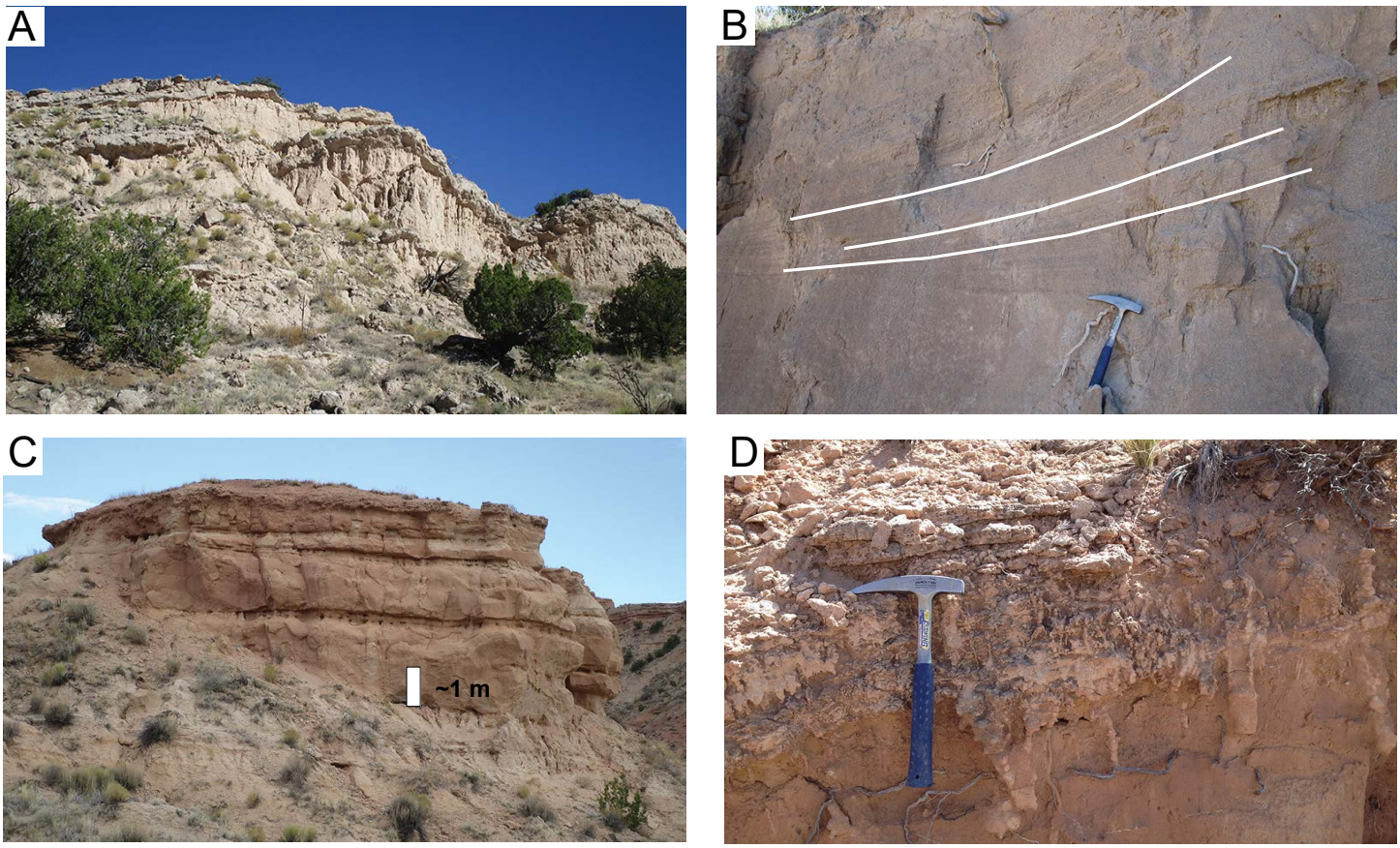



Figure 8. Photographs illustrating various members of the Zia Formation. (A) Bluffs underlain by the Piedra Parada Member; topographic relief is ~15–20 m. (B) Cross-stratification is common in the Piedra Parada Member. Here, foresets are tangential, face east (left in the photo), and are about 1 m tall (these foresets are partially annotated via white lines). Rock hammer for scale. (C) Upper strata of the Chamisa Mesa Member, which is generally composed of fine- to medium-grained, light-orangish sandstones in medium to thick, tabular beds. (D) The Chamisa Mesa Member is typically capped by a 0.5- to 1.5-m-thick, well-cemented, very fine- to medium-grained sandstone bed. Here, this interval is bioturbated (burrows and/or rhizoliths), mostly in its lower part. *Figure 8 continues on p. 13.*

are present in the sandstones (Fig. 8H; Koning et al., 2026c, fig. 2.27). The sandstone beds are mostly very fine- to medium-grained but locally contain sparse, very thin lenses of medium- to very coarse-grained sandstone. Lower contacts are generally sharp. Most of the beds have upper contacts that are relatively abrupt and planar but locally show gradational features, including (1) increased claystone laminations in the upper ~10 cm of the underlying sandstone bed and (2) the lower few decimeters of the overlying claystone are sandy but grade upward into purer clay (Koning et al., 2026c, fig. 2.26). However, some of the sandstone beds exhibit scoured upper contacts.

The proportion, geometries, and lateral relations of sandstone beds are informative. These sandstones are most abundant in the northeast end of the outcrop. Here and elsewhere, sandstone tongues taper laterally and interfinger with claystone-dominated strata (Koning et al., 2026c, figs. 2.24 and 2.25). In interfingering zones, sandstone beds may contain distinct claystone interlaminations (Fig. 8H). Sandstone-filled paleochannels are sparse, relatively small (roughly <1 m tall and <7 m wide), and observed mostly to the northeast. Locally, small channels are backfilled with clay (Koning et al., 2026c, fig. 2.28). Paleoflow directions are inferred from sandstone cross-stratification and lateral fining in sandstones intertonguing with clays. Two measurements indicate a southwest paleoflow direction (Fig. 4), and two localities to the north show east-northeast paleoflow (Koning et al., 2026c, station 3 of stop 1).

### *Geochronology*

An 80-cm-thick, fine, white tuff mixed with silt and very fine sand was sampled 3.0–3.3 m below the top of the unit and interpreted as fluvially reworked (sample SF-125-161026-djk in Fig. 6). The tuff yielded an $^{40}Ar/^{39}Ar$ age of 18.36 ± 0.14 Ma (Table 1, Fig. 3C), based on the five youngest concordant ages, and provides a maximum age constraint for the Cañada Pilares Member.

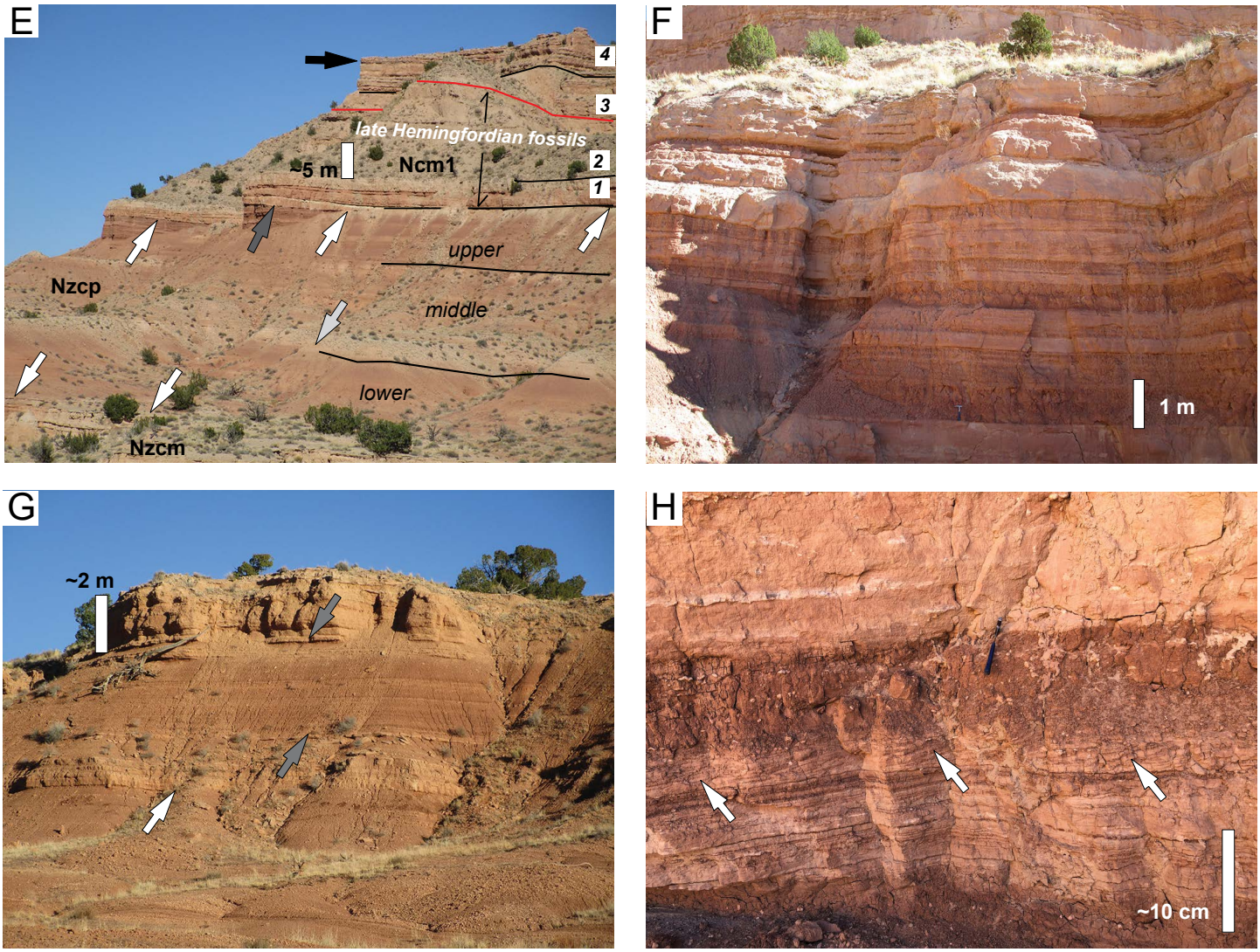



Figure 8 (continued). (E) The entire 38-m-thick section of the Cañada Pilares Member (Nzcp) is exposed between the two sets of opposing white arrows. Locally, it can be subdivided into clay-dominated, lower and upper units and a sand-dominated middle unit (see also stop 1 write-up in Koning et al., 2026c). Above lies the mixed-provenance unit of the Cerro Conejo Formation (subunit Ncm1), which can be further subdivided into four units per the Benavidez Arroyo-02 stratigraphic section (numbers in white squares denote stratigraphic section units AB-02-01 through AB-02-04). The white bed near the top-middle white arrow is inferred to transition laterally to a green mudstone. Note how the sandstone demarcated by the dark-gray arrow fills a paleochannel with ~1.5–2 m of basal paleotopographic relief. This sandstone, in turn, was eroded and on-lapped by the whitish mudstone and then by reddish-brown sandstone. The red line marks the tentative location of the main unconformity (cf. Fig. 6). (F) The upper contact of the Cañada Pilares Member varies from being sharp and scoured (as in panel E) to transitional or gradational; the latter is illustrated here in an exposure in Arroyo de Benavidez. (G) Intertonguing Cañada Pilares and lower Cerro Conejo Formations. The lower sand tongue (above the white arrow) thickens to the northeast (over hundreds of lateral meters) at the expense of thinning of the upper clay tongue (between the opposing gray arrows). Photo taken near 35°16' N, 106°54' W. (H) Intricately interlaminated clay and silt–very fine sand in the gradational upper contact of the Cañada Pilares Member at Arroyo Benavidez. View is to the east. Note cross-bedding of such strata (white arrow) capped by <1 cm of topset lamina, interpreted to be a low bar with foresets facing north-northeast and indicating a weak paleocurrent in that direction.

## *Cerro Conejo Formation*

The Cerro Conejo Formation consists of very pale-brown to pink to reddish, medium to thick, tabular-bedded sandstone with minor clayey sandstone–sandy claystone; this unit locally contains intervals dominated by cross-stratification (Connell et al., 1999). This unit frequently forms cliffs and ledges in the landscape. This formation was initially proposed as a member of the Zia Formation (Connell et al., 1999) but was later raised to formation rank (Connell, 2008b). The Cerro Conejo Formation overlies either the Chamisa Mesa or Cañada Pilares Members of the Zia Formation, depending on location. At the type section, the base is interpreted as an unconformity beneath a distinctive, ledge-forming interval of tabular-bedded sandstones, clayey sandstones, and mudstones (Connell et al., 1999; Connell, 2008b). The Cerro Conejo Formation generally underlies the distinctive, conglomeratic, light-yellowish-brown to pale-brown Navajo Draw Member of the Arroyo Ojito Member.

In the study area, the Cerro Conejo Formation is 300–330 m thick. Here, there is an informal stratum called the "green marker bed" that consists of a laterally continuous, greenish interval (a few meters thick) of mudstone, siltstone, fine sandstone, and minor limestone. This marker bed is located about 95 m above the base of the Cerro Conejo Formation and allows a stratigraphic tie between the Arroyo Benavidez stratigraphic sections to the north (Fig. 6) and Southern Boulevard section to the south (Fig. 7).

Beds in the Cerro Conejo Formation are tabular, but locally broad (typically >30 m wide) channel-fill geometries are observed. The sand fraction of the Cerro Conejo Formation ranges from very fine to very coarse but is predominantly fine- to medium-grained. Sand composition in the study area ranges from lithic arkose to subarkose (Koning et al., 2021a), with 40–70% quartz, 10–40% plagioclase and potassium feldspar, and 10–35% (typically 10–20%) mafic and lithic grains, including chert, volcanic fragments, and siltstone–fine sandstone detritus.

We divide the Cerro Conejo Formation into three mappable lithostratigraphic units corresponding to inferred depositional environments and provenance (associated map-unit labels are in parentheses): a northern-fluvial unit (Ncn), a western-piedmont unit (Ncw), and a mixed-provenance unit (Ncm), the latter representing complex mixing or interbedding between the other two (Figs. 2, 4, and 9). Contacts between these units are gradational and conformable.

### Northern-Fluvial Unit (Ncn)

The northern-fluvial unit is mapped in the Navajo Draw drainage, where it interfingers with and grades westward into the western-piedmont unit (northern part of Fig. 5). The sediment consists of light-gray, pink, and very pale-brown sandstone in ill-defined, medium to thick, lenticular to broadly lenticular beds ≤20 m wide (Figs. 10A and 10B). Locally, channel forms are evident (Fig. 10A). Within beds, the sandstone is structureless, horizontal-planar laminated, or cross-laminated with 20-cm-thick foresets commonly dipping at low angles. At some localities, and in close stratigraphic association with trough cross-stratification, minor clay-silt beds and intraformational conglomeratic sandstones are present, consisting of rip-up clasts of claystone, siltstone, and calcium carbonate-cemented sandstone. Cigar-shaped concretions produced by groundwater flow (Mozley and Davis, 1996) are oriented to the south (Fig. 5, northeastern corner). Groundwater flow was influenced by the sedimentary fabric and likely mimicked the paleotopographic surface. Thus, the southward orientation of these linear features and the location of the study area in the northwest corner of the Albuquerque Basin imply a southward-sloping basin floor during or shortly after deposition of the northern-fluvial unit.

The sandstone in the northern-fluvial unit is moderately to well sorted and mostly medium-grained (but ranges from fine to coarse). Relatively coarse sand (0.3–1.0 mm) occurs as outsized grains within finer sand or as distinct, lenticular laminae or very thin to thin beds. Trace reddish paleosols (~20 cm thick) are present, characterized by an estimated 5% clay accumulation, massive texture, and weak ped development. Pebbles were locally observed by the interfingering contact with the western-piedmont unit in the Navajo Draw drainage; here, pebbles consist of chert, granite, 1–3% quartzite, and trace rhyolite.

### Western-Piedmont Unit (Ncw)

The western-piedmont unit interfingers with and progrades over the other Cerro Conejo stratigraphic units. In its upper part, the western-piedmont unit is also referred to as the "upper red unit" of the Cerro Conejo Formation. Stratigraphic-structural relations near the western extent of the unit indicate it extends farther downsection to the west (Fig. 4, site C; Fig. 9; Koning and Rawling, 2017). In the Navajo Draw drainage, the western-piedmont unit interfingers eastward with the northern-fluvial unit (Figs. 5 and 9). To the south, the western-piedmont unit interfingers eastward with the mixed-provenance unit (Fig. 9).

Strata associated with the western piedmont unit are typically redder than northern-fluvial unit strata and exhibit slightly poorer sorting. Colors range from light orange, pink, and light brown to strong brown and reddish yellow–yellowish red (Figs. 11A–C). Sandstone beds are commonly 0.3–2 m thick and tabular and are structureless or exhibit laminations (horizontal-planar to low-angle cross-laminated). Measured paleoflow indicators are few (n = 5) and range from east to south (Figs. 4, 5, and 12). Beds locally exhibit both fining-upward and coarsening-upward trends. Where the western-piedmont unit progrades over older strata, there are commonly 10–20% mudstone and clayey sandstone beds near the basal contact (e.g., Fig. 7, near 65–70 m). Sandstone intervals are typically fine- to coarse-grained (mostly medium-grained), subrounded, moderately sorted, and composed of quartz, minor feldspar, and 10–20% lithic grains. The moderate sorting reflects the presence of coarse to very coarse sand grains (generally composed of chert) scattered in very fine- to medium-grained sand. Coarse sandstone may also form thin lenses (up to ~3% of exposure area). In the lithic fraction, chert exceeds volcanic grains by a factor of 2 to 3. Associated with the sandstone are trace to 15% beds of reddish and clayey, <30-cm-thick, tabular,

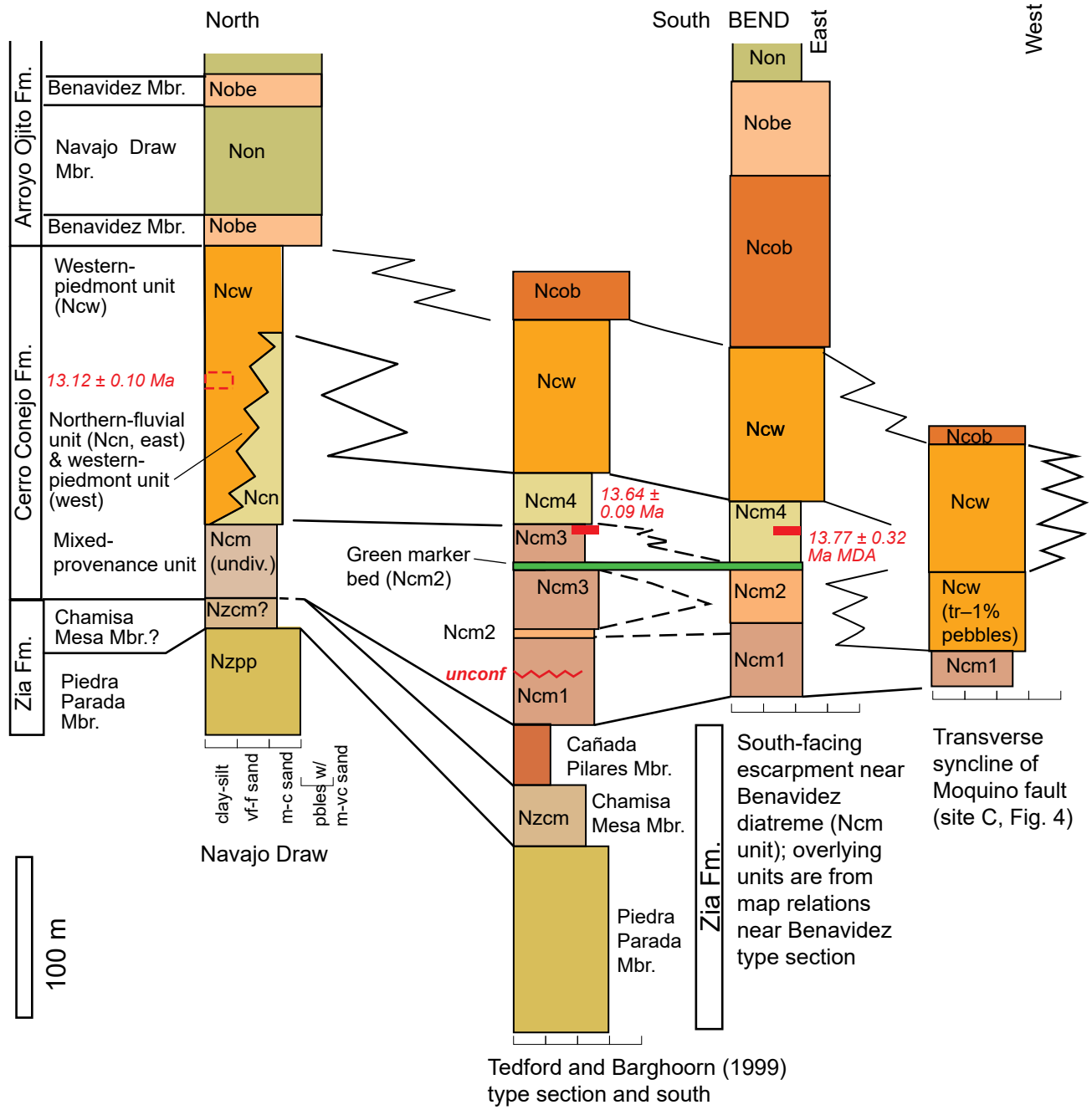



Figure 9. Stratigraphic correlation diagram showing thickness and unit changes of the lower–middle Santa Fe Group. From left to right in the diagram: Navajo Draw southward to 3 km northeast of Benavidez diatreme area, and from there westward to the transverse syncline on the Moquino fault hanging wall (Fig. 4, site C). The line of correlation is also shown in Figure 1. Red rectangles illustrate age control for the Cerro Conejo Formation (dashed where stratigraphic position is approximate).

very fine- to medium-grained sand that locally define bedding breaks (e.g., Figs. 11A and 11B; Fig. 7, 65–70 m in the Southern Boulevard stratigraphic section). Relatively common paleosols exhibit reddish cambic horizons and weak calcic horizons. Some reddish horizons are clay-enriched, although whether this enrichment is soil-related remains uncertain. Both soil horizon types feature weak to moderate, subangular blocky peds. Rhizoliths are locally present.

**Mixed-Provenance Unit (Ncm)**

The mixed-provenance unit (Ncm) can be divided into four provisional subunits that are difficult to map because of complex mixing and interfingering, although locally the subunits can be recognized and mapped (Fig. 4). The subunits are Ncm1, Ncm2, Ncm3, and Ncm4. Paleodepositional environment interpretations for each subunit are given below and synthesized in the Discussion section.

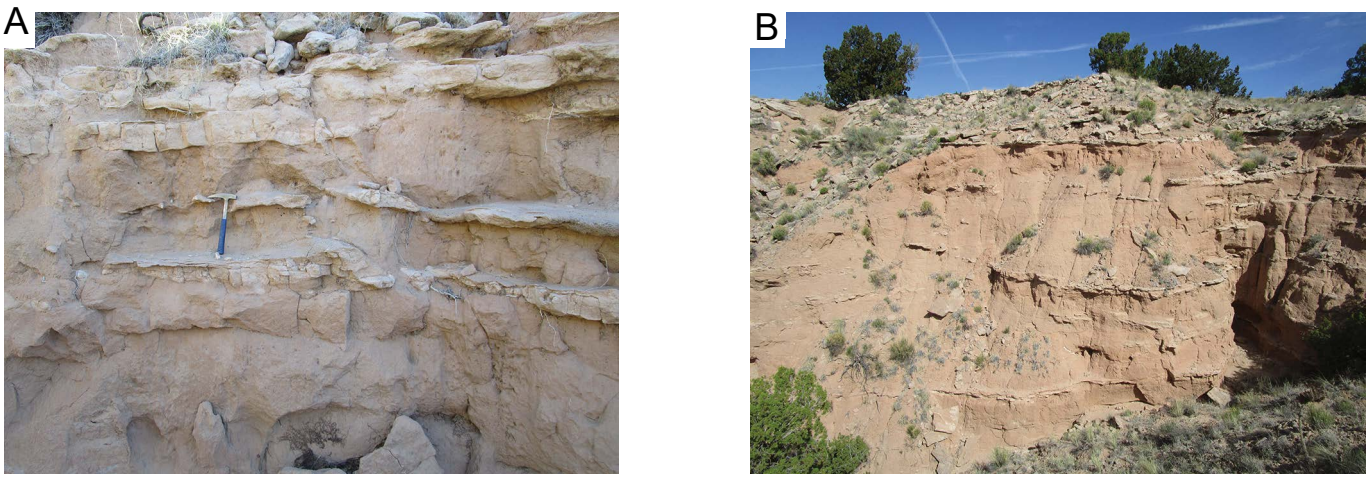



Figure 10. Photos in the Navajo Draw drainage of the northern-fluvial unit of the Cerro Conejo Formation. Here the unit is composed of tan to pink sandstone in vague, thin to thick, lenticular to broadly lenticular beds (up to 20 m wide) composed of fine- to coarse-grained (mostly medium-grained) sand. (A) Cementation accentuates the lenticular nature of the bedding. Rock hammer for scale. (B) Note the lack of fine-grained deposits in this ~10-m-thick exposure.

***Subunit Ncm1***

The lowest subunit, Ncm1, is a ledge-forming, well-bedded, tan to reddish sandstone at the base of the Cerro Conejo Formation that is 45–50 m thick (Figs. 6, 13A, and 13B; Appendix 1D, units AB-02-01 through AB-02-3). It is relatively continuous across the study area and capped by strongly cemented strata assigned to the lower tongue of Ncm2 (the latter shown in Fig. 4). Strata are mostly in medium to thick, tabular beds (Figs. 13A and 13B). These beds exhibit horizontal-planar laminations or cross-laminations (with tangential foresets up to a few meters thick) or are structureless. Sandstone is mostly very fine- to medium-grained, locally coarse-grained, and pink to light brown to reddish yellow. Minor (~10%) light-reddish-brown to reddish-yellow beds of claystone, siltstone, and very fine- to fine-grained sandstone are present.

The inferred depositional environment is a mixed fluvial-eolian setting. The presence of broad channel forms indicates fluvial deposition, but thick stratification sets are interpreted to be eolian. Structureless sandstone beds can be due to rapid deposition under uniform flow conditions, perhaps as a steady hyperconcentrated flow or else by bioturbation (e.g., roots or burrows).

***Subunit Ncm2***

Subunit Ncm2 is overall finer-grained and more thinly bedded than the other mixed-provenance subunits and, to the south, exhibits pastel colors (ranging from light greenish to grayish green to pink). The Benavidez Ranch fauna (late Barstovian North American Land Mammal Age [NALMA]) were mainly retrieved from this subunit (Morgan and Williamson, 2000, 2007). Subunit Ncm2 consists of very fine- to medium-grained sandstone, minor siltstone, and 5–10% claystone, mudstone, or clayey sandstone (Figs. 13C–13E). Sands are pink, pale brown, light gray, or white. Claystone beds may exhibit reduced or oxidized colors. The thickness of this unit ranges from a few meters to 30 m. In the south, the subunit thickens eastward.

Near our stratigraphic sections, subunit Ncm2 occurs as two tongues, the lower is ~6 m thick and the upper 2–5 m thick (units AB-02-04 through AB-02-05 in Fig. 6 and Appendix 1D; 0–5 m stratigraphic height in Fig. 7 and units SB-01 through SB-02 in Appendix 1C). In both tongues, beds are very thin to thick (mostly 3–50 cm) and tabular, and locally coarse sand is present. Sandstones in the lower tongue are well cemented (Fig. 13B, unit AB-02-04; Fig. 13C) and very fine- to coarse-grained but well sorted within individual beds (e.g., very fine- to fine-grained sandstone or medium- to coarse-grained sandstone). The cementation enhances visibility of sedimentary structures, revealing well-laminated (tabular to wavy) sandstones and locally abundant rootlets. The strong cementation results in an erosion-resistant cap on top of Ncm1 (Figs. 13A and 13B). The lower tongue hosts an important track locality (NMMNH L-4635) about 1.4 km west-northwest of the Benavidez diatreme. These tracks include those of a large borophagine dog, horse, camel, and proboscideans (mastodon or gompothere); these fossils are consistent with a late Barstovian (Ba2) NALMA (Morgan and Williamson, 2007).

A laterally extensive, ~2-m-thick, greenish clay and sand bed in the upper tongue of Ncm2 is interpreted to be a lacustrine or playa-lake facies (Fig. 13D). This bed is remarkably laterally extensive in a north-northeast direction (8–9 km) and is the green marker bed (Fig. 4). It contains large stromatolites and driftwood fragments. Locally, 10 m beneath the marker bed is a lower greenish, fine-grained bed that contains numerous fossils of the semiaquatic beaver *Eucastor* (Tedford and Barghoorn, 1999).

Compared to the northern-fluvial unit and its inferred correlative to the south (Ncm4), discussed below, subunit Ncm2 is lithologically distinct. Specifically, Ncm2 has notably more floodplain deposits (particularly to the south-southeast), local lacustrine deposits, sparser lenticular bedding, and finer-grained sandstones in thinner beds. This subunit also contains distinct channels and associated cross-stratification (with foresets up to

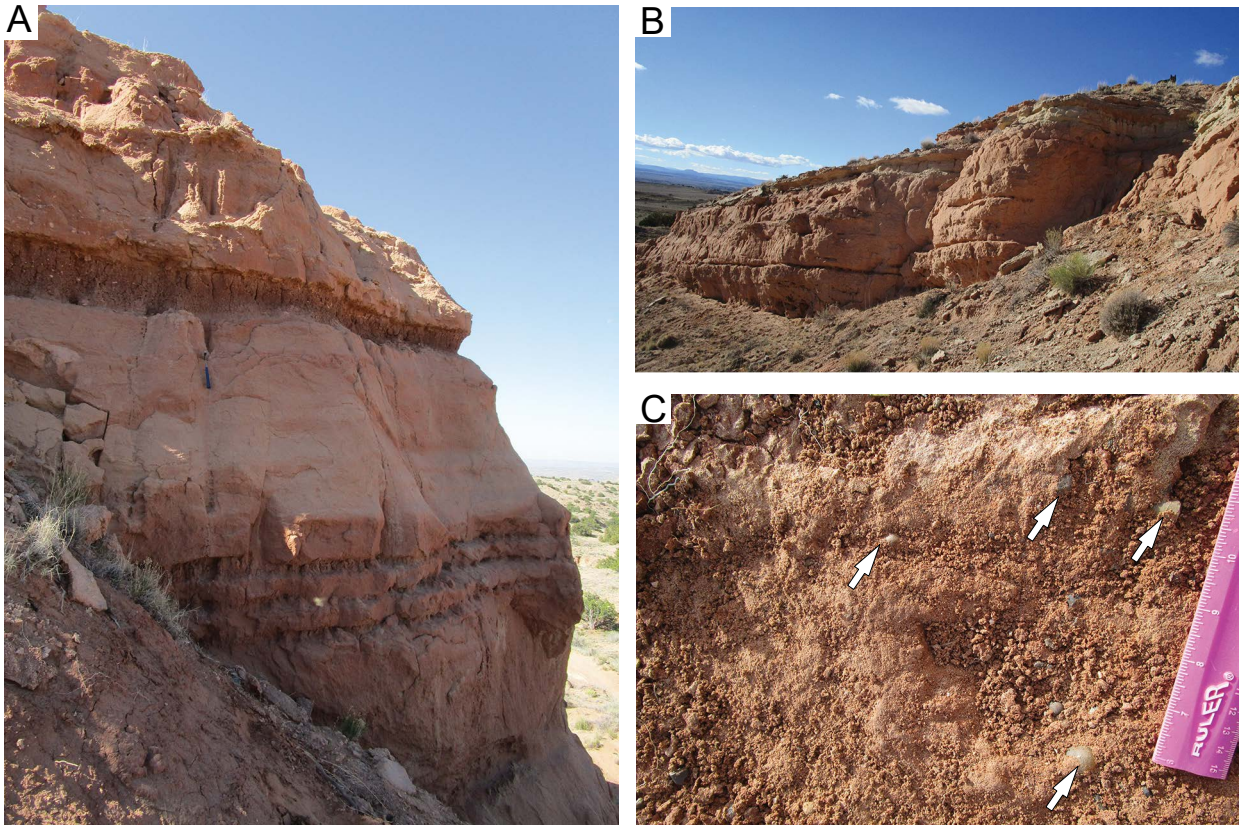



Figure 11. Photographs of the western-piedmont unit of the Cerro Conejo Formation. (A) Interbedded, reddish-yellow sandstone with 5–7% thin to medium, tabular, clayey, very fine- to medium-grained sandstone beds that form recesses in the outcrop. The thicker sandstone beds are medium to thick, tabular, and fine- to coarse-grained (mostly fine- to medium-grained). (B) Reddish, western-piedmont unit strata found about 35 stratigraphic meters above the base of the Cerro Conejo Formation. Most beds are thick and tabular, and the sandstone is moderately sorted and fine- to coarse-grained. (C) Interpreted debris-flow or hyperconcentrated-flow sediment near "C" of Figure 4. Note the granules and fine pebbles, which are not seen in correlative Cerro Conejo Formation strata to the east. This westward coarsening is consistent with this sediment being in a more proximal position on the piedmont.

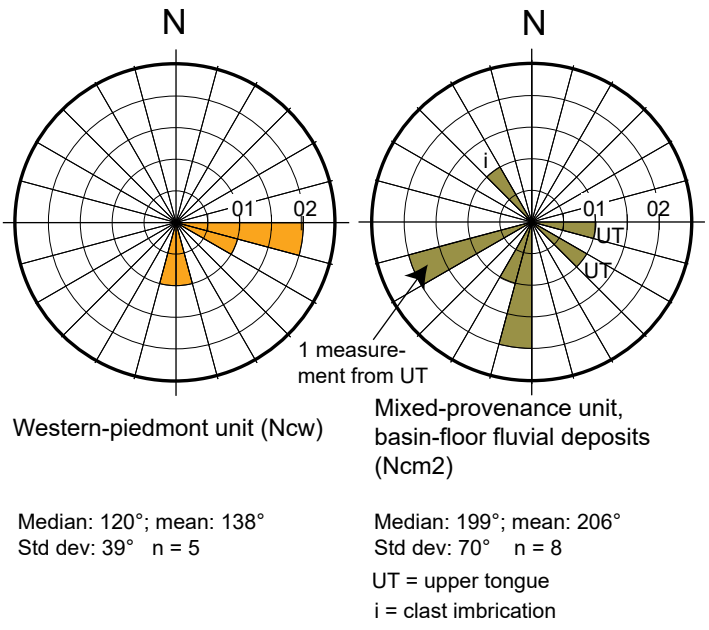



Figure 12. Stereonets illustrating paleoflow measurements in the Cerro Conejo Formation of the western-piedmont unit (left) and subunit Ncm2 (right) of the mixed-provenance unit (Appendix 3A). "UT" annotations in the Ncm2 plot denote those measurements from the upper tongue of Ncm2; remaining measurements are from the lower tongue of Ncm2. Measurements are from cross-stratification combined with channel margins; one measurement is from clast imbrication (labeled "i" in the Ncm2 plot). Depicted data do not include measurements from cigar-shaped concretions.

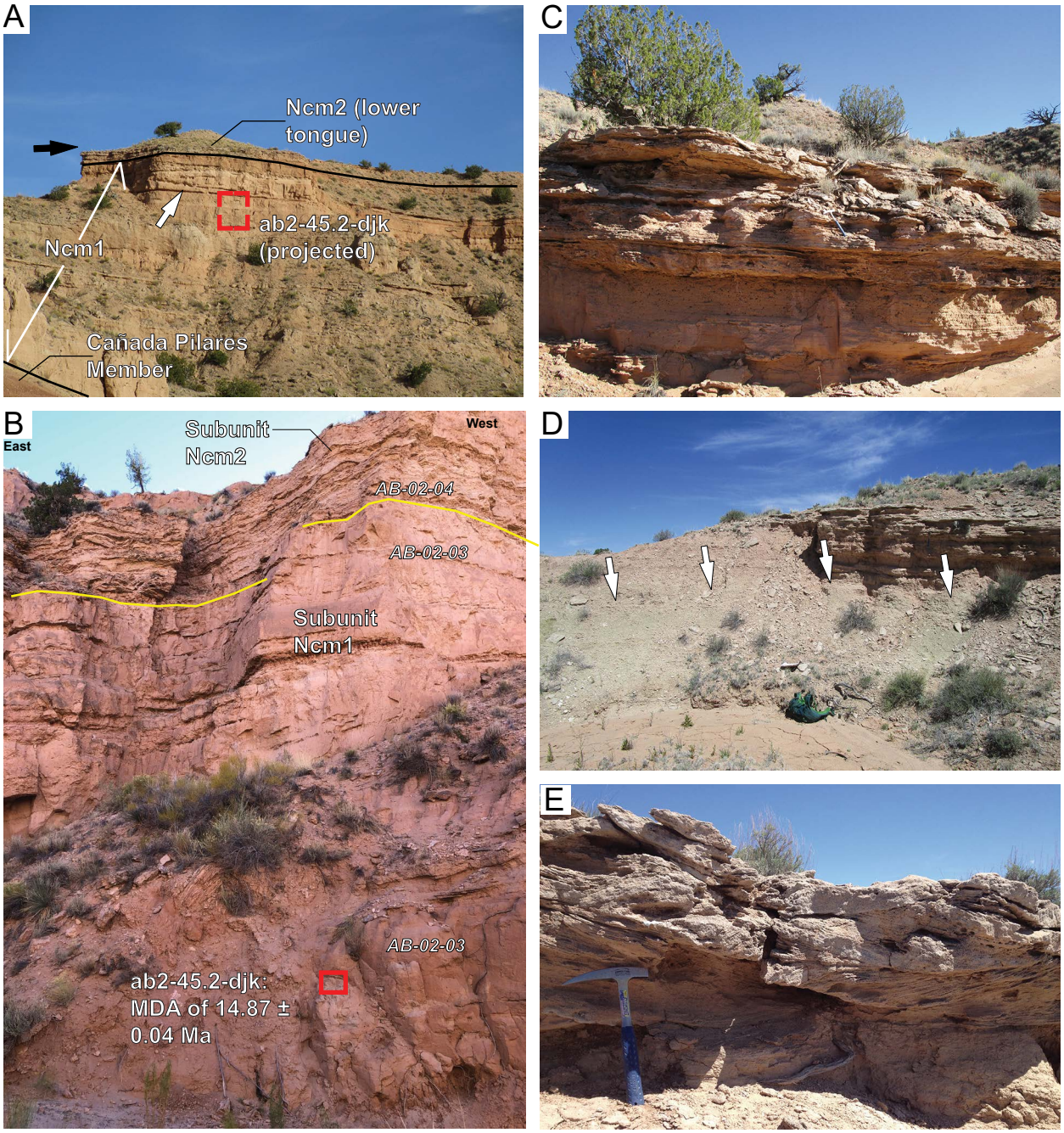



Figure 13. Photographs of three subunits of the mixed-provenance unit. (A) Typical appearance of subunit 1 (Ncm1), which makes up the lower 50–55 m of the formation. This unit exhibits a light-orangish to tan color and is composed primarily of sandstone in medium to thick, tabular beds. Near the white arrow, note the wedge-shaped ends of thick sandstone beds, consistent with fluvial deposition in broad paleochannels. Tabular, strongly cemented, very thinly to thinly bedded sandstone at top of the cliff is correlative to subunit 2 (Ncm2). (B) Subunit Ncm1 overlain by subunit Ncm2 in the Arroyo Benavidez-02 stratigraphic section. The location of the sand sample that gave the maximum depositional age of 14.87 ± 0.04 Ma is shown by the red square. Labels AB-02-03 through AB-02-04 are the stratigraphic section units detailed in Appendices 1 and 2. (C) Lower tongue of subunit Ncm2 of the mixed-provenance unit, consisting of tabular, laminated to very thinly bedded sandstone with high degrees of cementation by calcium carbonate. (D) Green lacustrine mudstone of subunit Ncm2 (below white arrows), which is ~1–2 m thick and laterally extensive across the northern two-thirds of the main map area (Fig. 4). Backpack for scale. Locally, two such mudstones are present, but the upper is the more laterally extensive and referred to as the green marker bed. Note the overlying tabular-bedded, laminated to very thin sandstone lithofacies similar to that seen in AB-02-04 of photo B (but the two are not time-correlative). (E) Trough cross-stratified sandstone locally found in subunit Ncm2.

20 cm thick; Fig. 13E), confirming it is a fluvial deposit. The channel fills are as thick as 2 m, commonly fine upward, and locally contain intraformational conglomerate (with cemented sandstone pebbles). General paleoflow ranged from southeast to southwest, overall more southerly than that of the western-piedmont unit (Fig. 12, Appendix 2). The tabular, thinly bedded, sandy nature of the lower tongue, which extends north–south across the study area, suggests deposition as a sheetflood system on the basin floor adjoining fan toes. The lack of soils and well-preserved bedding suggests rapid sedimentation and/or avulsion rates.

The green marker bed of the upper tongue of Ncm2 is composed mainly of mudstone and very fine- to fine-grained sandstone with light-grayish to light-greenish colors. Locally, the green marker bed has a basal limestone precipitated on a scoured, lower surface. The greenish sediment grades upward into a few meters of pink to light-brown, very fine- to fine-grained sandstone and mudstone inferred to be floodplain deposits, which in turn grade up into medium-grained sand interpreted as a distal piedmont lithofacies (Appendix 1C, Southern Boulevard section, units 1 through 2). This vertical stratigraphic succession and properties of the green marker bed (i.e., clay-rich texture and limestone) indicate a lacustrine environment on a south-trending (and south-sloping) floodplain.

### *Subunit Ncm3*

Subunit Ncm3 occurs both below and above the upper Ncm2 tongue (Figs. 6 and 9). This unit consists mainly of thick to very thick, relatively tabular beds of tan to pink to light-brown, fine- to medium-grained sandstone. Locally, beds coarsen upward. Massive sandstone is also present and is up to 9 m thick. Weakly developed paleosols are relatively common and correlate to 10- to 40-cm-thick Bw and 10- to 100-cm-thick Bk horizons; the Bk horizons are characterized by disseminated and nodular calcium carbonate. This unit is relatively similar to the western-piedmont unit, except that it is less red and more tan, and the majority of this unit may be related to the western piedmont or the transitional area between the distal piedmont and the basin floor.

### *Subunit Ncm4*

Subunit Ncm4 is characterized by fine- to medium-grained sandstone (mostly medium-grained) in poorly defined, medium to very thick, tabular to broadly lenticular beds. The unit's thickness ranges from 23 to 45 m, but the lower contact is notably gradational with subunit Ncm3, making thickness estimates difficult. Within beds, cross-stratification is sparse and, where present, the foresets are low-angle. The sand in these thick beds is mostly structureless or else horizontal-planar laminated to very thinly bedded. Very sparse paleosols are present and are characterized by reddish Bw or weakly developed Bt horizons. To the south, there are trace amounts of very thin to thin beds with very coarse sand and fine pebbles composed mainly of rhyolite–andesite with 10% chert and ~10% quartz. Interbeds of reddish mudstone, clayey sandstone, and fine- to medium-grained sand increase in proportion (but are still minor) downsection and laterally to the south. Cementation features are common in this unit, occupying 1–15% of the outcrop area and occurring as nodules, flattened concretions, cigar shapes, or 10- to 100-cm-thick, tabular to lenticular layers. This subunit is lithologically similar to the northern-fluvial unit mapped in Navajo Draw and is inferred to be a southward extension of that assemblage (Fig. 9). Both are inferred to be deposited by a southward-flowing fluvial system.

## Geochronology

At a stratigraphic height of 45.2 m above the basal contact of the Cerro Conejo Formation, a detrital sanidine sample was collected (ab2-45.2; Fig. 6). From this sample, we analyzed 195 detrital sanidine grains. Based on the two youngest concordant grains, a maximum depositional age of 14.87 ± 0.08 Ma was calculated (Table 1, Fig. 3D). We agree with earlier workers (e.g., Tedford, 1981; Tedford and Barghoorn, 1999) that a major unconformity (or perhaps a condensed section with several disconformities) representing ~2 Myr is present within ~30–45 m above the base of the Cerro Conejo Formation (Fig. 6). This interpretation is based on the 14.87 Ma maximum depositional age of sample ab2-45.2, the late Hemingfordian fossils (~18–17 Ma; Tedford and Barghoorn, 1997, 1999) in the lower ~30 m of the Cerro Conejo Formation (as defined in this work), and the lack of early Barstovian fossils (~16–15 Ma) in the Ceja del Rio Puerco region (Tedford, 1981, 1982; Tedford and Barghoorn, 1997, 1999).

Three radiometric analyses of sanidine from volcanic tuff(s) samples collected at ~120 m above the basal contact of the Cerro Conejo Formation, coinciding stratigraphically with 25–28 m above the green marker bed in the upper tongue of subunit Ncm2, provide a critical chronostratigraphic tie to the GPTS (Figs. 6 and 7). The first sample (BR-154-140122), collected 1 km north of the Benavidez diatreme (Fig. 4), was analyzed by single-grain $^{40}Ar/^{39}Ar$ dating of seven sanidine crystals. Most grains yielded inherited ages around 38 Ma, whereas the youngest grain produced an age of 13.77 ± 0.32 Ma, providing a maximum depositional age constraint for the tuff (Table 1, Fig. 3E). The second analysis (Tedford and Barghoorn, 1999) reported a 13.64 ± 0.09 Ma K/Ar age for a tuff at the same stratigraphic level; note that this age overlaps within uncertainties with the youngest $^{40}Ar/^{39}Ar$ sanidine from BR-154-140122.

The third sample, 4S-27.7, was collected from fine, biotite-bearing, white tuff 27.7–27.9 m above the green marker bed in the Southern Boulevard stratigraphic section (Fig. 7), at a similar stratigraphic level as BR-154-140122. Fifty sanidines were analyzed; the youngest grain yielded an age of 23.03 ± 0.08 Ma (Table 1, Fig. 3F). This age is inconsistent with the 14–13 Ma age constraints obtained from other samples in the lower–middle Cerro Conejo Formation and is interpreted as a maximum depositional age that is notably older than the depositional age. The large age dispersion observed for this sample indicates significant reworking and/or incorporation of inherited grains (as interpreted for aforementioned Zia Formation tuffs), with all dated grains being inherited rather than being primary phenocrysts reflective of the true depositional age. Based on the biotite-phyric nature of the tuff and the 13.6 Ma age constraints from nearby

samples, we suggest this tuff may correlate with the Pojoaque white ash of the Tesuque Formation in the eastern Española Basin (Koning, 2002; Spaur et al., 2025).

The youngest volcanic tuff bed was sampled in the Navajo Draw drainage (SF-77-161017-djk; Fig. 5), but its stratigraphic relation relative to the other tuffs is poorly constrained. Map relations and trigonometric calculations suggest that it lies approximately 80 m below the top of the Cerro Conejo Formation (Fig. 9). Four multigrain $^{40}Ar/^{39}Ar$ analyses (~10 crystals each) were performed. One analysis provided an older age of 13.70 ± 0.07 Ma, most likely reflecting the presence of one or more inherited grains. The remaining three aliquots overlap within uncertainties and define a robust weighted mean age of 13.12 ± 0.10 Ma (Table 1, Fig. 3G).

## *Arroyo Ojito Formation*

### Benavidez Member (Revised)

The Benavidez Member is a conglomeratic unit that is common west of the Rio Puerco and north of Interstate 40. This unit is generally an orangish-tan, medium- to coarse-grained sandstone with notable proportions of conglomeratic beds. The Benavidez Member was introduced and described by Koning et al. (2021a), who interpreted this unit as being deposited by east- to southeast-flowing, basin-margin paleodrainages during exhumation of the southeastern Colorado Plateau in the Miocene. In that work, this unit was proposed as an informal-rank member of the Cerro Conejo Formation.

In this paper, we propose a type section for this member (Fig. 14, Appendix 1A) and formally assign it to the Arroyo Ojito Formation. A criterion of ≥1% gravelly beds is used to distinguish the unit from the Cerro Conejo Formation, which has no gravel. In the study area, the Benavidez Member interfingers with the lower Navajo Draw Member and also with western-piedmont sandstones of the Cerro Conejo Formation (Figs. 4, 9, and 14). The coarser sand size, redder color, and chert-rich, relatively rounded gravel distinguishes this unit from typical strata of the Navajo Draw Member of the Arroyo Ojito Formation (note, however, there is abundant chert in the Navajo Draw Member near their associated contact).

Conglomeratic strata west of the Rio Puerco can be differentiated into a chert-gravel petrosome and subordinate volcanic-gravel and mixed-gravel petrosomes (Koning et al., 2021a). Paleoflow measurements are generally eastward-southeastward (Koning et al., 2021a), ranging from northeast to south (060° to 170°). Paleocurrent and descriptive details of the western Benavidez Member are found in Rawling and Koning (2019, 2020) and Koning et al. (2021a).

East of the Rio Puerco, including at the type section (Appendix 1A), the Benavidez Member is typically a reddish-yellow to light-brown to tan (collectively an orangish-tan) sand with common (≥1%) conglomerate beds (Fig. 14). Individual gravel beds are mostly very thin to thin and tabular to lenticular; pebbly sand is typically horizontal-planar laminated (Fig. 14). Gravel is dominated by rounded to subrounded, poorly to moderately sorted pebbles (ranging from very fine to very coarse) with <5% cobbles. Clasts are composed mainly of chert with minor (<10%) quartz, quartzite, sandstone (mainly eroded from Cretaceous strata), and petrified wood. Sandstone of the Benavidez Member is fine- to very coarse-grained (mostly medium- to coarse-grained), subrounded, moderately sorted, and composed of quartz, 5–12% dark grains (chert, mafics, volcanic grains), and 1–10% grains composed of orange-stained quartz, potassium feldspar, and granite (as estimated with a hand lens). Sparse calcic paleosols are present (<5% of unit) that feature reddening, subangular blocky peds, and 1–10% calcium carbonate nodules. Lamina to thin beds of reddish-brown clay to clayey sandstone are locally present, but these compose <3% of the exposure (Appendix 1A).

In the stratigraphically lower areas to the west (Figs. 9 and 11C), there are sparse (up to ~1% over ~10 m of stratigraphic thickness) pebble-bearing sandstone beds that are relatively thin (<10 cm) and commonly lenticular, as illustrated in the Alice King Bypass Road exposure (Fig. 4, site C; Appendix 1B). Here, there are up to 20% lenses (up to 10 cm thick) containing abundant coarse to very coarse sand grains and local pebbles. The pebbles consist of chert, 0.5–1% rhyolites–dacites, 2% vein quartz, 1–5% Proterozoic granite and gneiss clasts, 1–2% quartzite, and trace petrified wood.

### Navajo Draw Member

The Navajo Draw Member is at least 100 m thick on the footwall of the Sand Hill fault, which has excised the upper part of the member. The member consists of pale-brown to very pale-brown sandstone interbedded with intervals of mudstone and very fine- to fine-grained sandstone (Fig. 15). Conglomeratic intervals, typically pebbly channel fills (only 0.5–2% cobbles), are 30–100 cm thick and increase northward from ~10% to locally as much as 50%. Clast composition is dominantly chert and reworked tan sandstone (mainly intraformational or older Santa Fe Group sandstone). North of Navajo Draw, the gravel fraction becomes increasingly volcanic-rich (dacite–andesite), with minor chert and minor sandstone resembling Cretaceous strata (cf. Connell et al., 1999). Other clast types include 50% intraformational calcium carbonate nodules, iron-oxide fragments (inferred to be siderite reworked from Cretaceous strata), 1–7% quartzite, 5–7% quartz, and 1% petrified wood. Chert interpreted to correlate to the Pedernal chert (due to splotchy to mottled white, gray, brown, and black colors) increases upsection from 0–15%, and granite also increases upsection from 0–3%. Navajo Draw Member sandstone not associated with conglomerates is mostly very fine- to medium-grained and occurs in medium to thick, tabular to lenticular beds that exhibit horizontal-planar laminations or cross-laminations. (Fig. 15B). Mudstone and very fine- to fine-grained sandstone intervals are typically light brown and clay-rich and occur as tabular, laminated to thin interbeds. Strata are weakly consolidated, with 1% moderate to strong cementation.

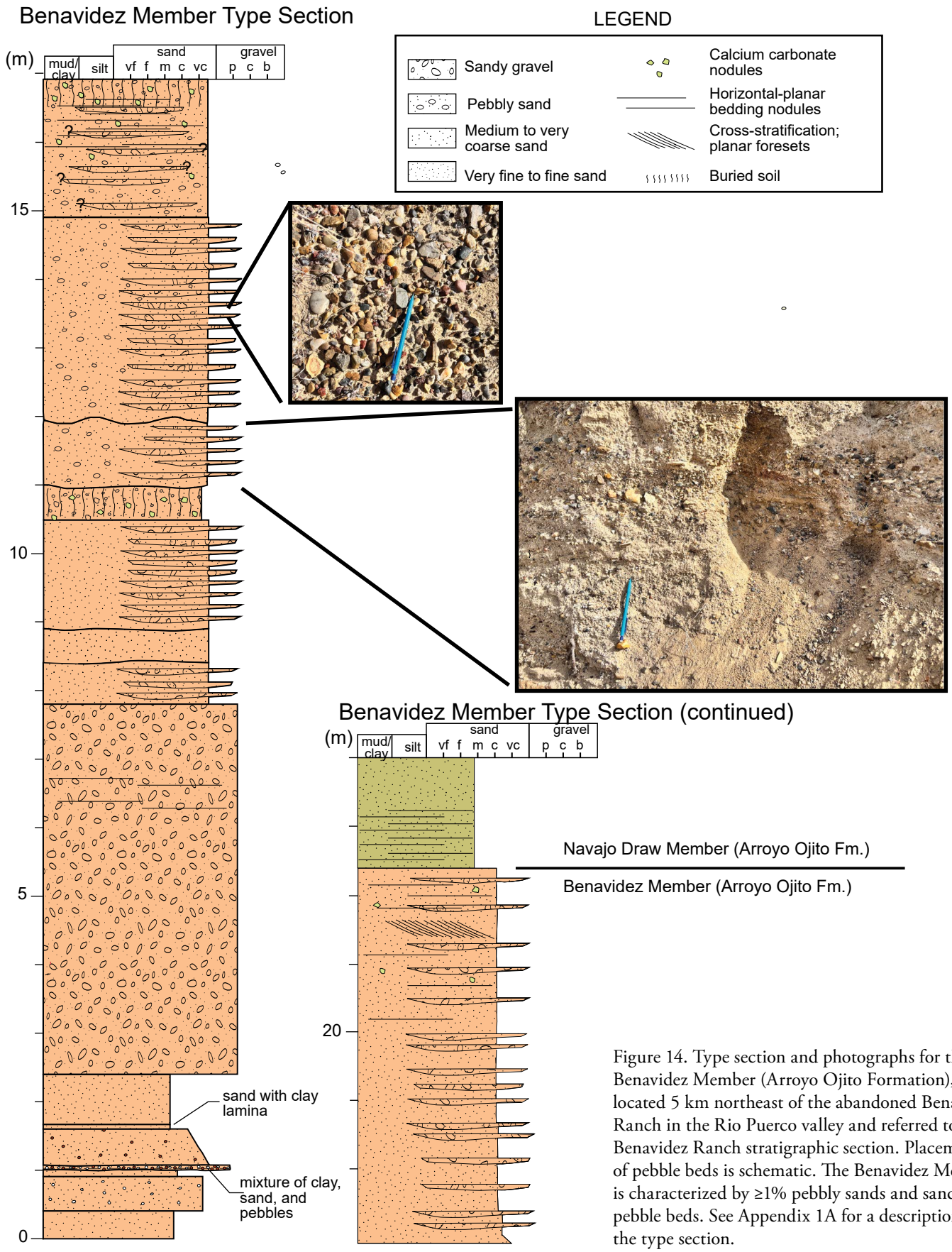



Figure 14. Type section and photographs for the Benavidez Member (Arroyo Ojito Formation), located 5 km northeast of the abandoned Benavidez Ranch in the Rio Puerco valley and referred to as the Benavidez Ranch stratigraphic section. Placement of pebble beds is schematic. The Benavidez Member is characterized by ≥1% pebbly sands and sandy pebble beds. See Appendix 1A for a description of the type section.

### *Detrital Sanidine and Provenance Investigation*

We used the 38–28 Ma population of detrital sanidine $^{40}Ar/^{39}Ar$ ages to investigate the provenance of two detrital sanidine samples (Fig. 6): AB-1.7-djk from the middle of the Chamisa Mesa Member (Zia Formation) and ab2-45.2 from the lower Cerro Conejo Formation (mixed-provenance unit). This evaluation was performed by comparing the detrital sanidine age distributions with the $^{40}Ar/^{39}Ar$ sanidine ages of many previously analyzed ignimbrites (and their source calderas) in the 38–28 Ma age range from the San Juan volcanic field (SJVF) and the Mogollon-Datil volcanic field (MDVF; Fig. 16). The ignimbrite sanidine data are derived from the New Mexico Geochronological Database that builds on the work of McIntosh et al. (1992), Lipman and McIntosh (2008), and Lipman and Zimmerer (2019). The two detrital sanidine samples exhibit age populations overlapping with ignimbrites from both volcanic fields (Fig. 16). The two samples contain detrital sanidine age clusters consistent with several MDVF ignimbrites, including the Datil Well, Kneeling Nun, Hells Mesa, and Bloodgood Canyon Tuffs. Both samples also have detrital sanidine clusters correlating to the Sapinero Mesa Tuff and Thorn Ranch Tuff of the SJVF. Interestingly, the stratigraphically higher sample ab2-45.2 has detrital sanidine that notably overlaps more with San Juan sources than does the AB-1.7-djk sample, including grains with ages matching the Blue Mesa, Grizzly Peak, and Fish Canyon Tuffs. Thus, sample ab2-45.2 appears to record a higher diversity and greater relative contribution of SJVF grains compared to sample AB-1.7-djk.

This observation suggests that the mixed-provenance unit of the Cerro Conejo Formation was sourced, in part, by a paleodrainage that reworked a larger component of SJVF detritus and likely extended farther north toward that region. This detritus was mixed with grains derived from the MDVF through fluvial and/or eolian processes.

### *Paleoclimate and Tectonic Proxies*

In the Discussion section below, we review the depositional history of the Santa Fe Group in the study area and preliminarily evaluate external forcings, mainly climate and tectonics, that may account for changes in deposition. Here, we examine proxies for these external forcings. Given the wide sampling intervals of the magnetostratigraphic data (Tedford and Barghoorn, 1999), interpretations presented here involve broad time intervals with boundaries that could change with future age control.

Stable isotope data collected and interpreted by Rugenstein et al. (2026) in the Ceja del Rio Puerco area provide a relevant paleoclimatic proxy for seasonality of precipitation: low $\delta^{18}O$ indicates predominantly wintertime moisture, whereas high $\delta^{18}O$ indicates summer moisture (Spaur et al., 2025). General trends and related interpretations from Rugenstein et al. (2026) include (1) low and steady $\delta^{13}C$ and $\delta^{18}O$ values during 20–17 Ma, consistent with high plant productivity and winter-wet precipitation; (2) steadily increasing values of $\delta^{18}O$ values from 14.8–12 Ma, consistent with increasing summer precipitation and related high-intensity precipitation events (Osborn and Reynolds, 1963; Drissel and Osborn, 1968; Etheredge et al., 2004); and

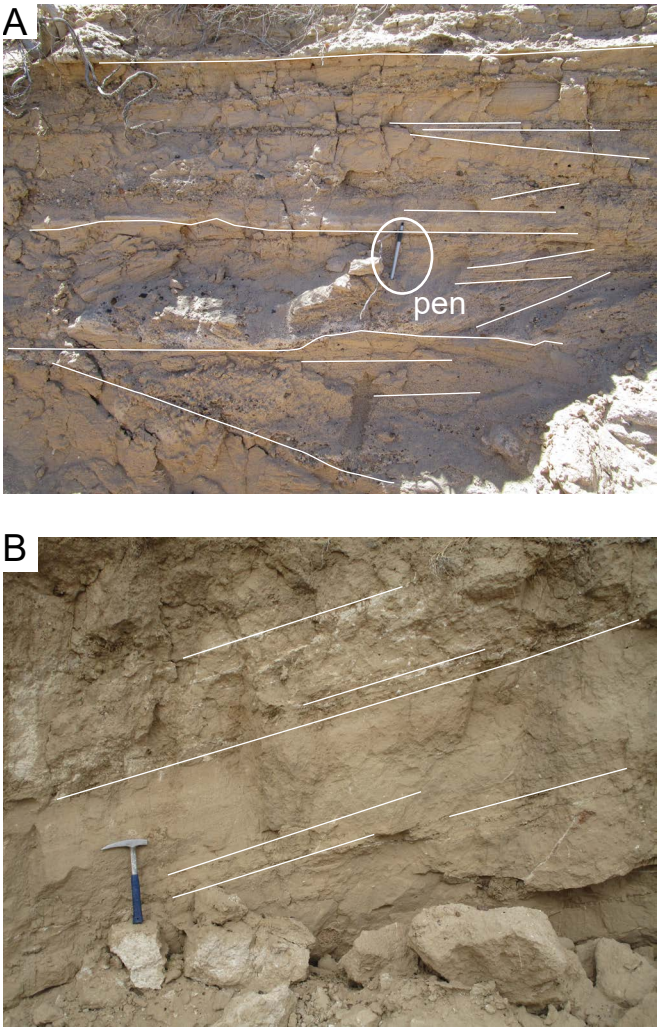



Figure 15. Photographs of the Navajo Draw Member of the Arroyo Ojito Formation. (A) Sand-dominated channel fills and sand sheets in 10- to 30-cm-thick, tabular to lenticular beds exhibiting horizontal-planar laminations or cross-laminations (the latter with planar foresets up to 15 cm tall). Bedding contacts and structures are indicated by white lines. Pen for scale. (B) Fine- to medium-grained sand interbedded with 2–3% very thin to thin, tabular clay beds. Here, bedding is tabular but dips to the left (indicated by white lines). Hammer for scale. These sandstones and claystones are likely floodplain deposits.

(3) relatively high $\delta^{13}C$ at 14.8–14.0 Ma that decreased between 14 and 12 Ma, consistent with a change from lower to higher plant productivity during 14–12 Ma and declining atmospheric $CO_2$ during this period (Cenozoic $CO_2$ Proxy Integration Project Consortium, 2023).

For an approximate tectonic proxy, we used relative changes in tectonic tilt rate (Fig. 17), calculated by plotting stratal dips in two locations, each corresponding to fault-bounded blocks with minimal internal deformation, north and east of the Benavidez diatreme: (1) between the Pilares and Moquino faults (but excluding the folded strata near Fig. 4 sites C, D, and E) and (2) the area bounded by the Pilares fault (to the west) and the Sand Hill fault (to the east). Stratal dips and their locations are

compiled in Appendix 3. Age-constrained stratigraphic intervals were binned, and the average and standard deviations for associated strata were calculated and plotted in the middle of the stratigraphic bin (in terms of the x-axis). Dips within ~50 m of a fault or in folded strata were excluded. Neighboring dips and strikes were found to be remarkably consistent in these two fault-bounded blocks (Fig. 4), and the overall east- to southeast-dipping structure south of Navajo Draw appears contiguous with regional eastward dips several kilometers to the east (Connell, 2008a, cross section B-B'; Grauch and Connell, 2013; Koning et al., 2026a, 2026b). The relative continuity of strikes suggests there are no localized compaction effects. Therefore, we interpret these dips as reflecting syntectonic regional tilting of this part of the Albuquerque Basin.

Changes in the average of the stratal dips in a bin divided by the related bin-mean ages gives stratal tilt rates (Appendix 3D). Tilt rates are ~0.6°/Myr between 17.7 and 14.4 Ma for the block between the Moquino and the Pilares faults. Tilt rates are similar for the block bounded by the Pilares and Sand Hill faults: 0.5–0.6°/Myr for the time period between 18.5 and 13.5 Ma. For the latter block, there are suggestions of changes in rates between the shorter-time bins within 17.7–13.5 Ma (Fig. 17), but these fall well within the one standard deviation error, so we do not elaborate on these, except we do note that between 13.5 and ~12 Ma the stratal tilt rate decreased from ~0.6°/Myr to 0.1°/Myr for the area between the Pilares and Sand Hill faults. In summary, a stratal tilt rate that encompasses data from both fault-bounded blocks is ~0.6°/Myr between 18.5 and 13.5 Ma. Projecting extrapolation of the lower tilt rates after 13.5 Ma to zero (modern day) gives a long-term tilt of ~0.3°/Myr, consistent with the possible lowering of rates to 0.1°/Myr between 13.5 and 12 Ma. Therefore, we interpret that tilt rates slowed after ~13.5 Ma (Fig. 17, Appendix 3D).

A proxy influenced by both tectonic subsidence and sediment flux are stratal accumulation rates (Fig. 17, blue line), calculated using our stratigraphic sections and associated age control (Figs. 6 and 7) and not adjusted for compaction (Appendices 4 and 5). Stratal accumulation rates were low to moderate (33–45 m/Myr) during 20–18 Ma (Piedra Parada and Chamisa Mesa deposition) and increased to 66 m/Myr during Cañada Pilares Member deposition (18.1–17.5 Ma). Above the lower Cerro Conejo unconformity,

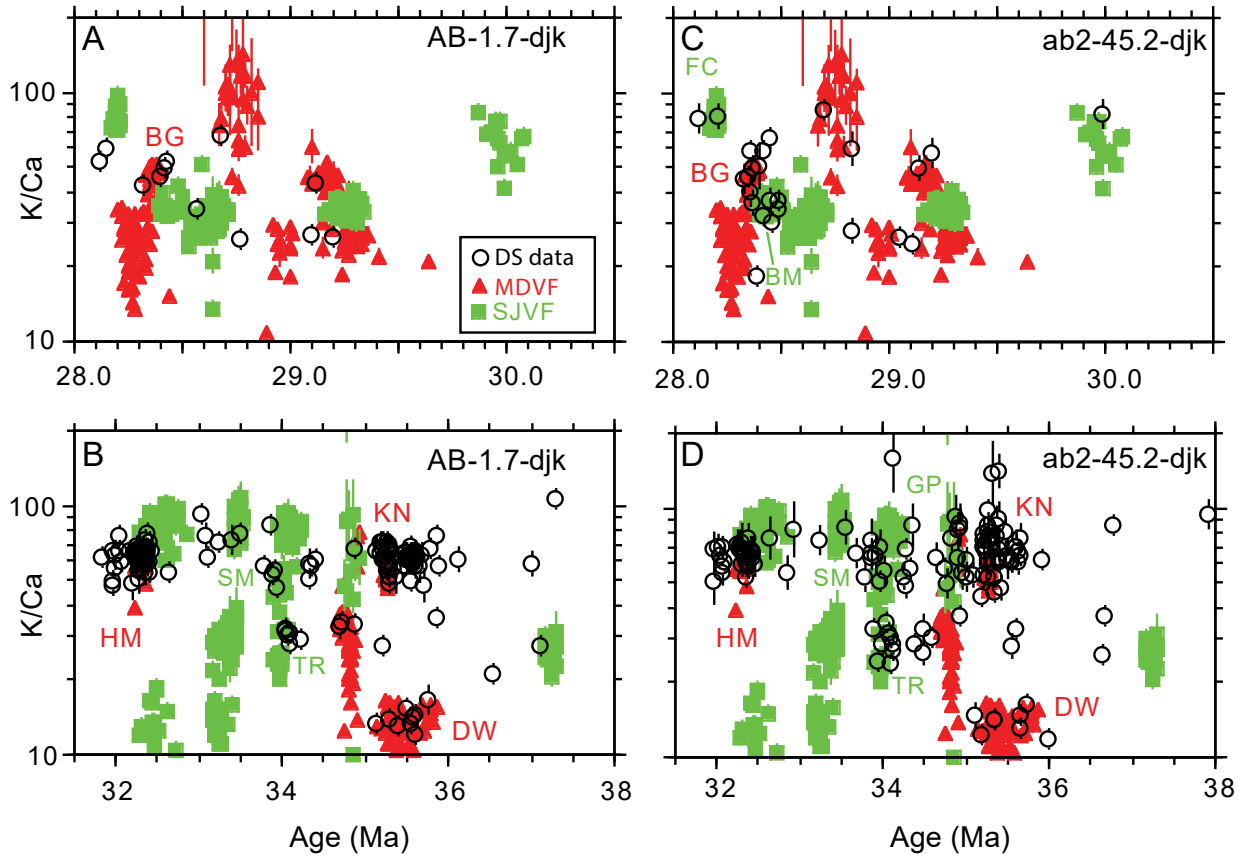



Figure 16. Plots showing age (Ma) versus K/Ca ratio for detrital sanidines from two sand samples: AB-1.7-djk (middle Chamisa Mesa Member of the Zia Formation, panels A and B) and ab2-45.2-djk (lower Cerro Conejo Formation, panels C and D). Detrital sanidine data are shown by open circles. Sandstone sanidine data are compared with sanidine results from ignimbrite samples erupted between 38 and 28 Ma, where red shades represent the Mogollon-Datil volcanic field (MDVF) and green shades represent the San Juan volcanic field (SJVF). Where there is an interpreted match between a group of detrital sanidine results and sanidine ignimbrite data, the match is labeled with the following abbreviations. In the MDVF: BG = Bloodgood Canyon Tuff, HM = Hells Mesa Tuff, DW = Datil Well Tuff, KN = Kneeling Nun Tuff. In the SJVF: FC = Fish Canyon Tuff, BM = Blue Mesa Tuff, SM = Sapinero Mesa Tuff, TR = Thorn Ranch Tuff, GP = Grizzly Peak Tuff. References for the MDVF and SJVF $^{40}Ar/^{39}Ar$ sanidine data for the ignimbrites are provided in the text.

stratal accumulation rates are high at 15–14 Ma (76 m/Myr). Rates were at moderate values (54–55 m/Myr) during 14–13 Ma and then decreased to 40–45 m/Myr at 13–9 Ma (Fig. 17, Appendices 4 and 5). Note that differences in correlations to the GPTS, especially for strata postdating 13 Ma, between our work and that of Tedford and Barghoorn (1999) lead to differences in stratal accumulation rates, with Tedford and Barghoorn (1999) interpreting relatively constant rates.

## Discussion

### *Paleoenvironments and Age*

#### Piedra Parada Member, Zia Formation

##### *Depositional Environment*

We agree with Gawne (1981a, 1981b) that the depositional environment for the majority of the Piedra Parada Member was eolian. Meter-scale cross-stratification is common in the unit, and the relatively large foreset heights (0.5 to >4.5 m), considerably thicker than in overlying strata, are more consistent with large eolian dunes than with fluvial dunes. Foresets generally dip eastward, indicating an eastward wind direction (Gawne, 1981a, 1981b). Concave-up channel forms with scoured bases and coarse-grained basal lags, expected in fluvial environments, are lacking. Broadly lenticular laminae are consistent with grain flows observed on modern eolian dunes. However, the presence of local pebbly beds to the southwest (west of the Rio Puerco; Fig. 1, site A) indicates interbedding of fluvial and eolian deposits in that area (Koning and Jochems, 2014). Given the similarity of the sandstone composition and the eastward paleowind direction, the associated fluvial system probably served as the primary source of the eolian sand in the study area (Fig. 18A).

##### *Age*

Studies of the mammalian biochronology (Galusha, 1966; Gawne, 1981a, 1981b; Tedford and Barghoorn, 1997, 1999; Tedford et al., 2004) constrain the age of the Piedra Parada Member to the latest Arikareean (Ar4) NALMA (21–19.0 Ma). We follow the revised biochronology for the Arikareean of Albright et al. (2008). Fossils mostly belong to camels (*Stenomylus*, *Oxydactylus*, and *Michenia*) and rhinos (*Diceratherium*). Note that the 21–19.0 Ma age from fossil data is consistent with the maximum depositional ages provided by four dates of the basal, volcanic gravel clasts. These ages include 33.7 ± 1.1 Ma (Table 2, Fig. 3H), 33.67 ± 0.24 Ma, 33.46 ± 0.02 Ma, and 32.2 ± 1.8 Ma (W.C. McIntosh and S.M. Cather, unpublished data reported in Connell et al., 2007; corrected for Fish Canyon Tuff standard of Kuiper et al., 2008). These ages are distinctly older than the 29.7–28.5 Ma ages obtained from andesitic–dacitic gravel clasts of the Gilman Formation in the southwestern Jemez Mountains (Kelley et al., 2013b), so we interpret the Piedra Parada gravel as being sourced from a different eruptive center.

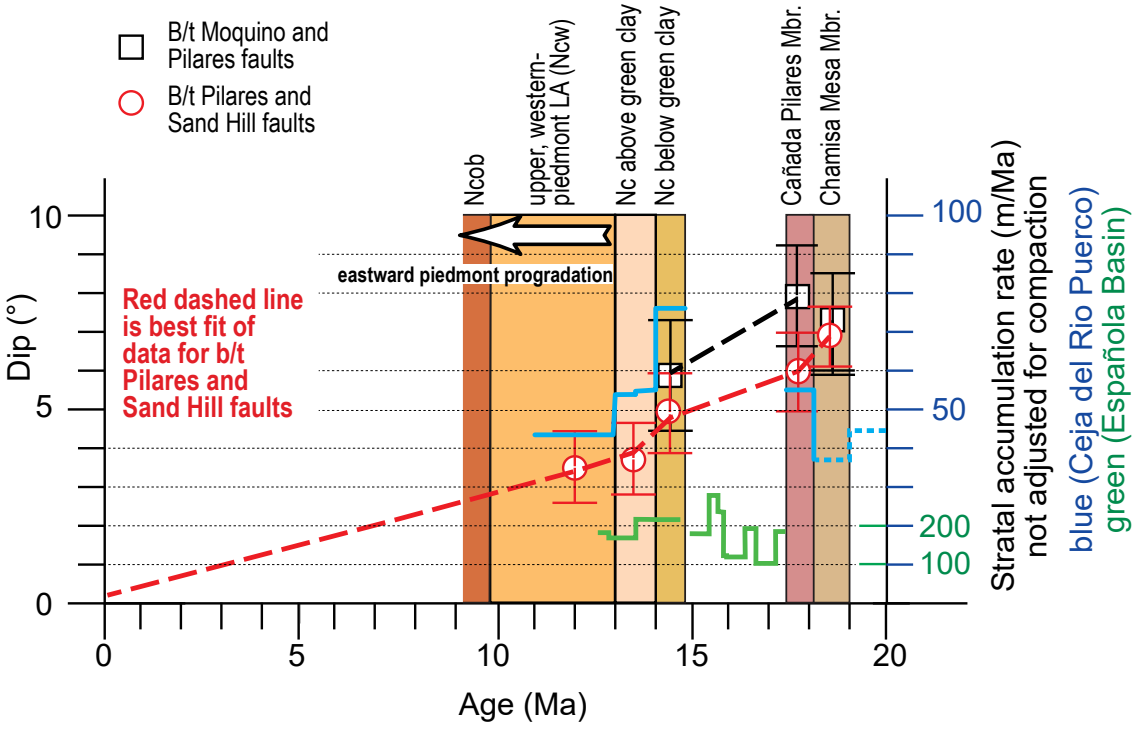



Figure 17. Average and standard deviation of stratal tilts collected in two fault-bounded blocks in the study area. For the more complete stratigraphic succession (between the Pilares and Sand Hill faults), a dashed red line connects the averages, and the slope of the line is equivalent to tilt rates (latter given in Appendix 3D). Stratal accumulation rates (Appendix 4) are shown as a blue line. For comparison, stratal accumulation rates from the Española Basin are shown in green (note the different scale); these data are from Spaur et al. (2025) and Koning et al. (2026d). Note how strata accumulation rates were relatively low in the Española Basin between 17 and 16 Ma, approximately coinciding with unconformity development in the Ceja del Rio Puerco study area.

**Chamisa Mesa Member, Zia Formation**

***Depositional Environment***

We infer the depositional environment of the Chamisa Mesa Member to represent a distal piedmont transitioning to a basin floor. Sandstone beds are tabular, suggestive of relatively unconfined fluvial sheetflow or eolian sand sheets (the latter being the preferred interpretation of Gawne [1981b] for strata in the lower–middle parts of the member). A paleochannel margin is oriented 151° and another paleocurrent is 195° (Appendix 2). Complimentary unidirectional data (e.g., channel plunge or imbrication) were not available, but an assumed south-southeast topographic slope is consistent with the study area's location along the western margin of the Albuquerque Basin. Cemented beds, especially in the upper part, exhibit various features consistent with deposition on moist ground or spring-mound deposits, which often occur at the toe of a piedmont. These include relatively fine laminations, porous to vuggy textures, and paleoburrows and rhizoliths.

***Fossils and Age***

Vertebrate fossils were collected only in the upper 5 m of the Chamisa Mesa Member and nearly all are the stenomyline camel *Blickomylus galushai* (Tedford and Barghoorn, 1999). At its type area on Chamisa Mesa (40 km to the north-northeast), this camel occurs with more abundant and diverse faunal remains, including rhinos, carnivores, rodents, and camels, that collectively indicate a temporal range of early Hemingfordian (He1) NALMA (Frick and Taylor, 1968; Gawne, 1981a, 1981b; Tedford, 1981). Gawne (1981a, 1981b) and Tedford and Barghoorn (1999) noted that fossils in the overlying Cañada Pilares Member are suggestive of the early Hemingfordian, the latter having a minimum age of 17.5 Ma based on Tedford et al. (2004). This constraint indicates that the Chamisa Mesa Member is also early Hemingfordian (within 18.9 to 17.5 Ma assigned to that NALMA age, per Tedford et al., 2004).

We evaluate the biochronologic age interpretation by (1) $^{40}Ar/^{39}Ar$ dating of sanidine in a detrital sandstone sample and in a tuff bed and (2) comparing these constraints against the magnetostratigraphic data of Tedford and Barghoorn (1999). The sandstone sample was collected 16 m below the upper contact and returned a maximum depositional age of 18.26 ± 0.06 Ma (Fig. 6, SB-1.7-djk), and the fluvially reworked tuff, sampled 2 m below the upper contact, yielded a maximum depositional age of 18.10 ± 0.46 Ma (Fig. 6, SF-115-161025-djk). These maximum depositional ages are consistent with the interpreted early Hemingfordian age for the vertebrate fossils.

In addition to yielding early Hemingfordian fossils, the upper two-thirds of the overlying Cañada Pilares Member has a reversed magnetic polarity (Fig. 6). In contrast, two magnetostratigraphic samples collected from near the base of the Cañada Pilares Member (one a few meters above and one just below the contact), returned normal polarity (Fig. 6). Given these constraints, the middle to upper Chamisa Mesa Member most likely correlates to chron C4En and has an age of 18.5–18.1 Ma. The basal, lower parts of the Chamisa Mesa would be slightly older, potentially up to 19 Ma, given the latest Arikareean fossils in the Piedra Parada Member.

**Cañada Pilares Member, Zia Formation**

***Depositional Environment***

The claystone-dominated nature of Cañada Pilares Member strata, coupled with its rift-basin setting, suggests two plausible depositional environments: floodplain or playa lake (the latter potentially within a broader floodplain). The green claystone and local limestone indicate standing water conditions at the top of the section. In contrast, most of the remaining clays lack indicators of persistent standing water (e.g., reduced, low-chroma colors or symmetrical ripple marks). Inspection of three samples did not reveal ostracods. The following observations support interpretation of a floodplain or small playa lake with a northeast-southwest axis in the proximal hanging wall of the Moquino fault: (1) absence of the Cañada Pilares Member in the Navajo Draw drainage (Fig. 5), (2) decreasing sandstone/mudstone ratio toward the southwest from the northeasternmost exposure of the member (presumably toward the center of a small paleotopographic depression), (3) notable westward thinning of the Cañada Pilares Member in western exposures, where it intertongues with sandstones (Fig. 4, site D), (4) common intertonguing and interlamination of sandstone beds with reddish-brown claystone (Fig. 8H, lower half), and (5) relative paucity of fluvial channels. Periodic standing water is supported by relatively high $\delta^{18}O$ values in authigenic carbonates sampled in this member as well as high $\delta^{18}O$ variance among samples from the Cañada Pilares, which is frequently interpreted as intermittent evaporation of shallow lakes that enriches authigenic carbonates in $\delta^{18}O$ (Dettmann et al., 2003; see data presented in Rugenstein et al., 2026). If this were a broad, flat floodplain with intermittent standing water, the primary fluvial channels would likely have been east of the study area since the unit's mudstones pinch out westward within distal-piedmont sandstone deposits (Fig. 4, site D).

***Fossils and Age***

The Cañada Pilares Member, particularly near the top of the unit, has yielded a diverse fauna that include remains of the rhino *Menoceras* cf. *M. marslandense* and the camel *Blickomylus galushai*. Gawne (1981b) and Tedford and Barghoorn (1999) interpreted this fossil assemblage to likely be early Hemingfordian, with a minimum age of 17.5 Ma (Tedford et al., 2004).

An 80-cm-thick, fine, white tuff, mixed with silt and very fine sand, was sampled 3.0–3.3 m below the top of the unit and interpreted as fluvially reworked (sample SF-125-161026-djk in Fig. 6). It yielded an $^{40}Ar/^{39}Ar$ maximum depositional age of 18.36 ± 0.14 Ma for the Cañada Pilares Member (Table 1, Fig. 3C) based on the five youngest concordant ages (Table 1, Fig. 3C). Given this maximum age constraint, the early Hemingfordian fossil assemblage, and the fact that the unit is mainly magnetically reversed (except for basal strata), the Cañada Pilares Member must correlate to one or both of chrons C5Dr.1r and C5Dr.2r (Fig. 6).

The younger age limit of C5Dr.1r is 17.533 Ma (Fig. 6), indicating that the top of the Cañada Pilares Member is as young as 17.5 Ma. The base of the member lies ~10 m below the inferred C5Dr.2r/C4En boundary (Fig. 6). We assign an age of 18.1 Ma to the base because it is older than the C5Dr.2r/C4En boundary (older than 18.0 Ma), but the maximum detrital age of sample AB-1.7-djk in the middle Chamisa Mesa Member indicates the base is younger than 18.3 ± 0.06 Ma (Fig. 6). Note that we use the maximum depositional age of AB-1.7-djk, rather than SF-115-161025-djk, because of the lower analytical error of AB-1.7-djk.

## Cerro Conejo Formation

### *Depositional Environment and the Tamaya Paleodrainage*

We interpret that the Cerro Conejo Formation in the Ceja del Rio Puerco represents deposition from two drainage systems (Figs. 18 and 19). These commonly intertongue and mix, accounting for mixed-sourced sand units described above (e.g., Ncm1 through Ncm3). The first system, associated with the northern-fluvial unit and subunit Ncm4 of the mixed-provenance unit, represents fluvial deposition on the distal parts of a broad megafan associated with a particularly large, ephemeral(?) river draining southeastward from the adjoining Colorado Plateau (Figs. 18B and 19). This megafan and associated river (or perhaps relatively closely spaced, parallel-flowing rivers), which we call the Tamaya paleodrainage, are described in more detail below. A lack of thick (>0.5 m) cross-stratification sets, the dearth of discontinuous, coarsening-upward lamina indicative of grainflows (Bristow and Mountney, 2013), and the paucity of frosted grains discount a widespread eolian environment, although minor proportions of eolian deposits (i.e., sand sheets and localized small dunes) are likely. A general fluvial paleoenvironment is indicated by the aforementioned channel forms, local intraformational conglomerates, and trace granules to pebbles. The relative absence of clayey strata is noteworthy and suggests relatively high-energy, voluminous, and episodic deposition, the latter likely being associated with avulsions. This inferred megafan would likely have sloped southward, based on the aforementioned measurements of linear, cigar-shaped sandstone cementation.

The second depositional system inferred for the Cerro Conejo Formation is interpreted as a distal piedmont depositional environment (Figs. 18B–D and 19). Paleoflow was mainly east-southeastward (Fig. 12, Appendix 3). The deposit grades westward and upward into pebble-bearing deposits of the Benavidez Member (Arroyo Ojito Formation), consistent with a prograding piedmont on the western margin of the Albuquerque Basin. Various sediment characteristics and the relatively thick, tabular beds are similar to those described in distal piedmont deposits present in the upper Santa Fe Group in the San Marcial and Palomas basins (e.g., Koning et al., 2018, 2020, 2021b). Comparable intrabed features include the absence of sedimentary structures except for horizontal-planar laminations, weakly developed paleosols, and moderate to poor sorting and clayey, very fine- to medium-grained sandstone inferred to be associated with hyperconcentrated flows (Seager and Mack, 2003, p. 78).

### *Fossils and Age*

We interpret the age of the Cerro Conejo Formation as ranging from ~17 to 9 Ma. According to Tedford and Barghoorn (1999), fossils in the lower 30 m of the unit are best assigned to the late Hemingfordian (17.5–16.2 Ma; Fig. 6). Above ~30 m, fossils in the middle part of the formation locally include the gomphothere or mastodon *Gomphotherium* and are correlated to the late Barstovian (Ba2) NALMA, with an age range of 14.8–12.5 Ma (Tedford and Barghoorn, 1999; Morgan and Williamson, 2000; Tedford et al., 2004). Information about what fossils, if any, may have been retrieved from the upper Cerro Conejo Formation has not been published.

The combination of the 14.87 Ma maximum depositional age of the detrital sanidine sample (ab2-45.2) and the 13.64 Ma tuff provides relatively well-constrained correlations to the GPTS (Fig. 6). Sample ab2-45.2-djk is from a normal interval, and the 13.6 Ma tuff occurs just above an inferred, relatively long normal-polarity interval that likely correlates to C5ACn or possibly a longer C5ACn through C5ADn interval. Below, the presence of two normal-reverse polarity pairs in the magnetostratigraphic data of Tedford and Barghoorn (1999) constrains the 14.87 Ma maximum depositional age and its associated normal polarity to the C5Bn.1n GPTS chron (Fig. 6).

Collectively, the $^{40}Ar/^{39}Ar$ data and GPTS correlations permit these provisional age constraints, subject to revision with future age control. Unit Ncm1 extends from the disconformity up to 14.8 Ma, the lower tongue of Ncm2 is 14.8–14.7 Ma, and the green marker bed is likely ~14.0 Ma, although the green marker bed could possibly be correlated to 14.6–14.5 Ma if the overlying normal-polarity strata are interpreted to C5ADn. Our preferred correlation of strata with the GPTS above the 13.6 Ma tuff indicates that the base of the western-piedmont unit in the Southern Boulevard section is ~13 Ma, and unit Ncm4 ranges from 13.5 to ~13 Ma (Fig. 7).

Our correlations of the upper Cerro Conejo Formation magnetostratigraphy to the GPTS (Fig. 7, >90 m) deviate from the correlations of Tedford and Barghoorn (1999) and will be the focus of additional detrital sanidine dating. In this section, we assume no missing chrons in the magnetostratigraphic data, and, given the lack of absolute age control in the upper Cerro Conejo Formation, this assumption could lead to miscorrelations with the GPTS. Our tentative correlations for the upper Cerro Conejo Formation, including where it interfingers with gravelly tongues of the Benavidez Member (defined below), suggest that the western-piedmont unit of the Cerro Conejo Formation is as young as 10–9 Ma, consistent with age interpretations of the upper contact reported by Connell (2008b).

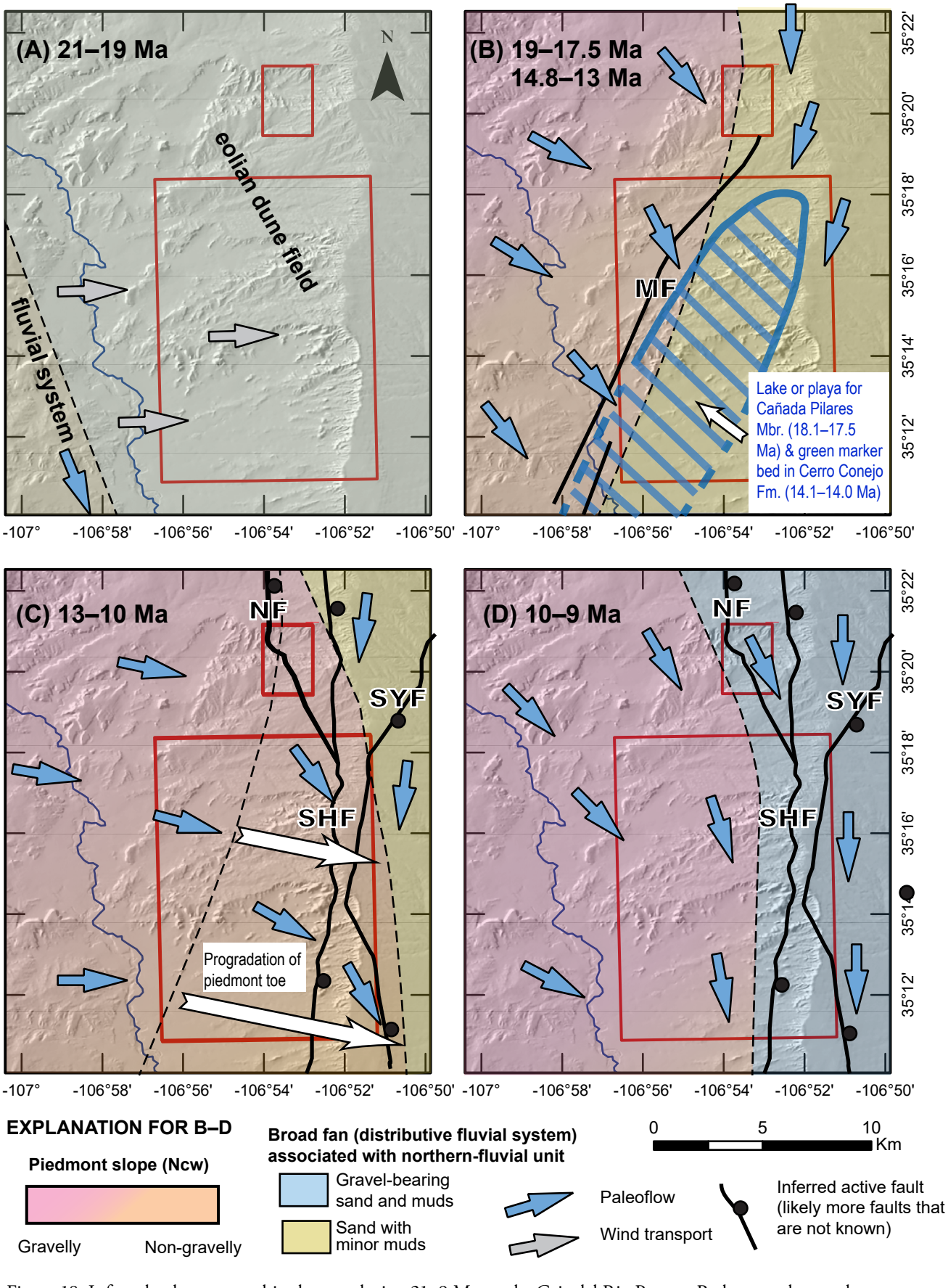



Figure 18. Inferred paleotopographic changes during 21–9 Ma on the Ceja del Rio Puerco. Red rectangles are the area covered by maps in Figure 4 (bottom) and Figure 5 (top). See text for discussion. Abbreviations on faults are MF = Moquino fault, NF = Navajo fault, SHF = Sand Hill fault, and SYF = San Ysidro fault. Modern topography is shown as a hillshade in order to provide spatial reference.

**Benavidez and Navajo Draw Members, Arroyo Ojito Formation**

***Depositional Environment***

Previous workers have interpreted the depositional environment of the Navajo Draw Member to be a braided-river system sourced in the southeastern Colorado Plateau (Connell et al., 1999; Connell, 2004). Our study corroborates that interpretation. Gravelly channel fills indicate fluvial deposition. The presence of laminated, medium to thick, tabular beds composed of very fine- to medium-grained sand are likely sheetflood deposits associated with fluvial depositional lobes. The brownish, well-sorted, thinly bedded, clay-rich mudstones to fine sandstones are interpreted as floodplain deposits. Paleoflow data from gravel-clast imbrication at three sites indicate a southeastward flow direction (southeastern part of map in Fig. 5). The presence of reworked chert, siderite, and Mesozoic sandstones further confirms a source from Colorado Plateau strata that were being eroded and transported down the Navajo Draw fluvial system.

We propose that the minor presence of quartz, quartzite, granite, and Pedernal chert (mainly <10% each), with the proportion of the granite and Pedernal Chert increasing upsection, supports the interpretation that the Oligocene Ritito Conglomerate was being reworked from the Nacimiento Mountains (see Kelley et al., 2013b, regarding Ritito Conglomerate) and fluvially transported into the Navajo Draw paleodrainage. The axis of the Tamaya paleodrainage would have been rerouted southward around this bedrock paleotopographic high. The emergence of the Nacimiento Mountains may be due to exhumation related to late Miocene epeirogeny (Cather et al., 2012) or perhaps it is driven by magma injection or heating associated with the Jemez Mountains volcanic field. The Benavidez Member was deposited on an east- to southeast-sloping piedmont by streams sourced in the southeasternmost Colorado Plateau. Additional discussion of the paleogeography and depositional history of the Benavidez Member is provided in Koning et al. (2021a).

***Age***

In contrast to the Cerro Conejo and Zia Formations, the Arroyo Ojito Formation is generally nonfossiliferous, and sparse radiometric dating outside the study area is used to constrain its age. The base of the Navajo Draw Member is interpreted to be ~10 Ma based on correlation of the uppermost Cerro Conejo tuffs (not seen in study area but present 27 km to the northeast) to the 11.3 Ma Trapper Creek B tephra (Koning and Personius, 2002; Connell, 2008a, 2008b; Koning et al., 2026b). In north-facing badland exposures about 15–20 km north-northeast of this study, northeast of La Ceja (Fig. 1), the Navajo Draw Member generally lies below a bed of the 7.0–6.9 Ma Peralta Tuff, present in the lower Loma Barbon Member (Koning et al., 1998; Connell et al., 1999; Connell, 2008b). However, above the Peralta Tuff bed, near La Ceja and immediately east of the San Ysidro fault, the Navajo Draw and Loma Barbon Members interfinger with each other, so the Navajo Draw is as young as 7–6.5 Ma on the proximal hanging wall of the San Ysidro fault. Due to erosion of the Arroyo Ojito Formation on the footwall of the San Ysidro fault (Connell

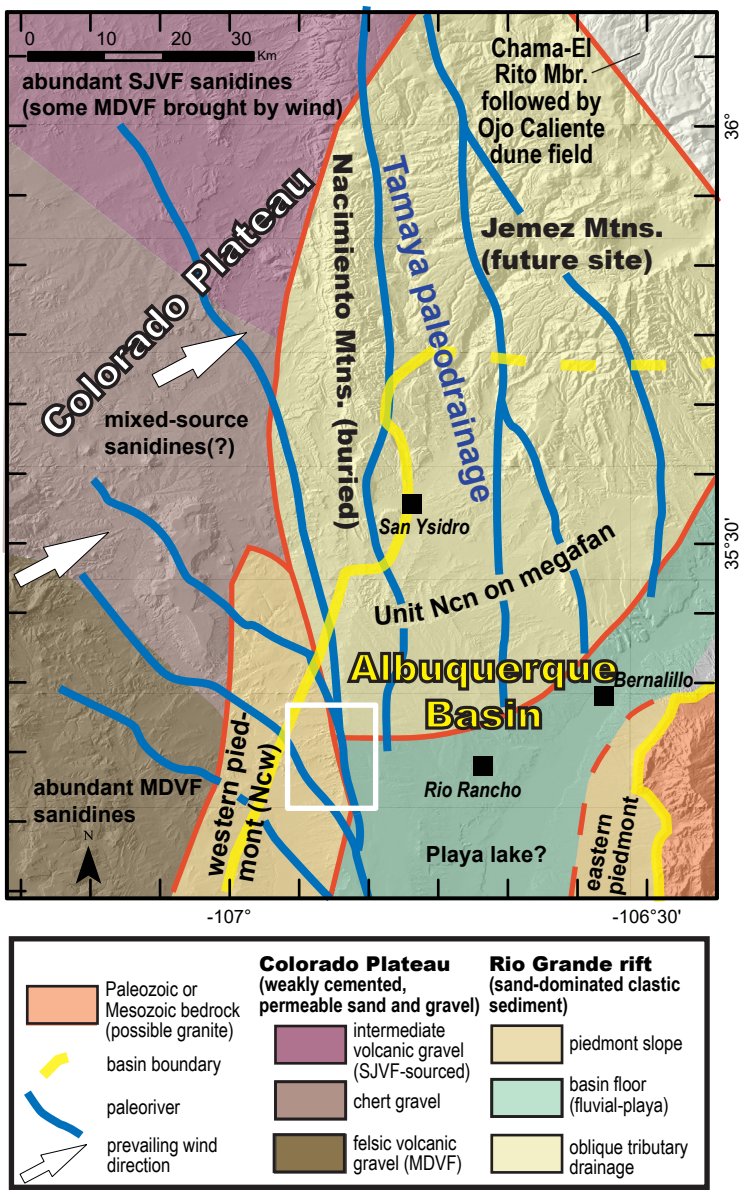



Figure 19. Paleogeographic map for the northern Albuquerque Basin and southeastern Colorado Plateau for 14–13 Ma. Modern topography is shown as a hillshade in order to provide spatial reference. Note that the Jemez Mountains formed after 10 Ma. The Nacimiento Mountains, initially formed in the Laramide (Cather, 2004), were buried by post-35 Ma sediment and were exhumed ~10 Ma. We interpret that ~10 Ma exhumation of the Nacimiento Mountains facilitated erosion of upper Eocene sediment (including the Ritito Conglomerate), and these clasts were transported into the 10–7 Ma Arroyo Ojito Formation (see text). SJVF = San Juan volcanic field, MDVF = Mogollon-Datil volcanic field.

et al., 2026), Navajo Draw outcrops would be older, perhaps ~8 Ma, but more work is needed to constrain the age of the Navajo Draw Member in the Ceja del Rio Puerco.

Preserved strata of the Benavidez Member are interpreted to be 13–10 Ma along the Ceja del Rio Puerco. However, the westward coarsening of lower Cerro Conejo Formation strata indicates that the Benavidez Member was likely present in the west by ~14.5 Ma (Figs. 4 and 9, site C; Appendix 1B). Correlations of the Southern Boulevard stratigraphic section to the GPTS indicate the base of the red upper unit (Ncw) is 13.0 Ma (Fig. 7). At the top of the Southern Boulevard section, correlating the position of the interbedded Benavidez and Cerro Conejo Formations (Ncbe) to the GPTS indicates an age of 10–9 Ma (Fig. 7). Therefore, progradation of the upper red unit (Ncw; Figs. 7 and 9), culminating with deposition of the Benavidez Member, occurred between 13 and 10 Ma. Reconnaissance data indicate that reddish, chert-dominated gravel underlies the northwest corner of the 8.11 ± 0.05 Ma La Mesita Negra basalt flow near I-40 (Fig. 1, site B; Cikoski et al., 2012; age of basalt from Maldonado et al., 2006). Thus, deposition of the Benavidez Member continued until at least 8 Ma. Comparing this age range with that of the Navajo Draw Member, discussed above, indicates the Benavidez Member interfingers eastward with most of the Navajo Draw Member of the Arroyo Ojito Formation. This interfingering is also partly observed at the Benavidez type section, where the Benavidez Member is overlain by fine-grained sandstone of the Navajo Draw Member (Fig. 14).

### *Unconformity in the Lower Cerro Conejo Formation*

A prominent intraformational unconformity at or near the base of the Cerro Conejo Formation has been inferred in the Ceja del Rio Puerco study area. Gawne (1981b) interpreted an angular unconformity at the base and recognized that the fossils of the early Barstovian NALMA were missing in overlying strata (her "age equivalent of Pojoaque Member of the Tesuque Formation"). The lack of early Barstovian (Ba1; ~16–14.8 Ma) faunas there, and also north of La Ceja in southern Zia Pueblo, was confirmed by subsequent paleontological investigations (Tedford, 1981, 2004; Tedford and Barghoorn, 1999; Morgan, 2015). We agree with Tedford and Barghoorn (1999) that the upper contact of the Cañada Pilares clays alternates between sharp and intertonguing. In our Arroyo Benavidez stratigraphic section, for example, the contact ranges from gradational (Fig. 8F) to sharp (Fig. 8E). An angular unconformity there was not noted, although local angular relations due to paleochannels are present (Fig. 8E). We do note a locale, 1.4 km west of the Benavidez diatreme and immediately adjacent to the Moquino fault (UTM coordinates 324,00 m E, 3,901,00 m N, zone 13), where there appears to be a slight angular unconformity (Koning and Jochems, 2014, fig. 14 of the report). But this may be a local phenomenon related to deposition immediately adjacent to the fault (implying the fault was active at ~18 Ma).

Sparse camel remains resembling late Hemingfordian forms were recovered (Tedford and Barghoorn, 1999) in the lower 30 m of what we map as the Cerro Conejo Formation, but these strata were assigned to a sandy, upper Cañada Pilares Member unit by Tedford and Barghoorn (1999). We agree with Tedford and Barghoorn (1999) that the main unconformity is probably best placed approximately 30 m above the base of the Cerro Conejo Formation (Fig. 6), as defined per our work. Rather than being a single unconformable surface, the time gap may instead comprise multiple disconformities distributed between 0 and 30 m above the base of the Cerro Conejo Formation. Alternatively, the 30-m-thick interval may represent a condensed stratigraphic section.

Additional geochronologic work using detrital sanidine is required to precisely constrain the location of this unconformity (or unconformities if more than one is present). Field investigations suggest the main unconformity may correlate with the boundary between the AB-02-02 and AB-02-03 stratigraphic units in the Arroyo Benavidez-02 section (Fig. 6). However, this contact is not a prominent outcrop feature: lithologic contrasts at the proposed level (~30 m) are subtle and difficult to trace confidently across kilometer-scale exposures.

The lacuna and possible degradational vacuity (pause in deposition and possible erosion, respectively; Wheeler, 1964) associated with the unconformity probably spans 17 to 15 Ma. A detrital sanidine maximum depositional age of 14.87 ± 0.08 Ma (sample ab2-djk, Fig. 6), collected 45 m above the top of the Cañada Pilares Member, indicates the presence of a stratigraphically significant lacuna below that sampled stratigraphic level. Fossil data and new radiometric data, coupled with reasonable correlations to the GPTS, indicate that the top of the Cañada Pilares Member likely corresponds to the 17.5 Ma C5Dn/C5Dr.1r chron boundary (Fig. 6). Based on fossil data, late Hemingfordian strata are likely present in the lower ~30 m of the Cerro Conejo Formation. Considering the reversal in the paleomagnetic data at ~17 m in the Arroyo Benavidez-02 stratigraphic section, possibly the 17.2 Ma C5Cr/C5Dn chron boundary, the youngest Hemingfordian strata may be ~17 Ma (Fig. 6). Collectively, these data indicate the intraformational unconformity likely spans a period of 2 Myr between 17 and 15 Ma.

Conceptually, it is often inferred that major disconformities coincide with formation boundaries. However, the North American Stratigraphic Code specifies that such contacts be based on lithostratigraphic criteria (North American Commission on Stratigraphic Nomenclature, 2005). Identifying the Cerro Conejo Formation base at the top of the underlying reddish-brown, clay-rich strata (the original definition of the Cañada Pilares Member of Gawne [1981a, 1981b]) results in a lithologic-based contact that can be readily reproduced among mappers along the Ceja del Rio Puerco.

### *Benavidez Member (Arroyo Ojito Formation)*

We designate a type section for conglomeratic strata that we formally propose as the Benavidez Member of the Arroyo Ojito Formation (Fig. 14, Appendix 1A). Previously, this unit was included within the Cerro Conejo Formation due to the similarity of the respective sand fractions (Koning et al., 2021a). However, here we redefine the member and formally include it within the Arroyo Ojito Formation because the conglomeratic character better matches the lithologic criteria for that previously defined formation (Connell et al., 1999; Connell, 2008b). The Benavidez Member intertongues with and grades laterally into the Navajo Draw Member of the Arroyo Ojito Formation in Ceja del Rio Puerco exposures (Fig. 5) and in the subsurface to the east (Koning et al., 2026a, 2026b). An interfingering/laterally gradational contact within the same formation is convenient for mapping purposes. Older (stratigraphically lower) Benavidez Member is present to the west, where it intertongues with the lower–middle Cerro Conejo Formation (Fig. 4, site C; Fig. 9; Appendix 1B). This illustrates a westward coarsening of the western piedmont, consistent with the predominantly eastward paleoflow of the western-piedmont unit of the Cerro Conejo Formation and the Benavidez Member to the west of the Rio Puerco (Fig. 12; Koning et al., 2021a).

### *General Paleogeographic Features*

After ~19 Ma, the general paleogeography of the larger study area consisted of a western, southeast-sloping piedmont bounded on the east by a gently southward sloping, broad fan (Fig. 19). This fan graded southward to a southerly sloping basin floor (Figs. 18B and 19). Sediment was derived primarily from drainages of the southeastern Colorado Plateau, consistent with southeast- to south- to southwest-directed paleoflow (Figs. 4, 5, 12, and 19; Koning et al., 2021a). During the Early Oligocene, sandy deposits correlative with the Chuska erg likely capped much of the southeastern Colorado Plateau (Cather et al., 2008). However, these sandstones intertongued with fluvial, gravelly fan deposits sourced from nearby paleotopographic highs (Koning et al., 2021a). Two of these fans originated from volcanic sources (Fig. 19). To the north was a south-sloping, volcaniclastic apron sourced from the southeastern San Juan volcanic field. To the south was a north-sloping, volcaniclastic apron sourced from the northeastern Mogollon-Datil volcanic field (Koning et al., 2021a). Between these two opposing fans was a chert-dominated, fluvial deposit likely shed from the Zuñi Mountains (Koning et al., 2021a) and carrying reworked chert sourced primarily from the Shinarump Formation (S. Lucas, written communication, July 13, 2026).

Since this chert-bearing unit has been completely eroded in the southeasternmost Colorado Plateau, confirmation of the degree of consolidation and cementation of the gravelly sand cap is difficult to determine. However, the fact that <1% of the gravel clasts in the Benavidez Member consist of intraformational sandstone suggests that most of the source area was weakly cemented and weakly lithified. Likely correlative strata to the west exposed near the Arizona–New Mexico border, the Chuska Sandstone, are locally well cemented but are intercalated with friable, weakly cemented eolian sandstone; the sandstone was remarkably permeable, with 26–42% pre-cement porosity (Cather et al., 2008). A likely correlative to the Chuska Sandstone in the deep subsurface of the Albuquerque Basin is the 486-m-thick unit of Isleta #2, consisting of up to 500-m-thick, well-sorted sandstone that is only locally cemented in its lower half (Connell et al., 2007; Cather et al., 2008). Based on these limited data, we infer that the gravelly sand-capping unit on the southeastern Colorado Plateau was well sorted and weakly cemented, with some intervals of strong cementation.

Another important paleogeographic feature was a broad fan complex (megafan) deposited by a south-southeast-flowing, relatively large paleodrainage defined here as the Tamaya paleodrainage (Fig. 19). The broad fan probably extended as far as 70 km to the northeast, at the approximate border of the Albuquerque and Española Basins (Koning et al., 2013, geology of St. Peter's Dome described in their appendix G), using outcrop-based correlations of lithologically similar sandstone. The relatively long distance perpendicular to the southeast paleoflow suggests an apex-to-toe length of >30 km. Consequently, this fan can be categorized as a megafan or large distributive fluvial system (Hartley et al., 2010; Weissmann et al., 2010). The proximal part of this megafan coincided with the southwestern and central Jemez Mountains, which had not yet formed. Northeast-directed prevailing winds likely blew sand from the Tamaya paleodrainage to the northeast, forming the Ojo Caliente Sandstone eolianite in the western Española Basin (Fig. 19; Galusha and Blick, 1971; Dethier and Manley, 1985; Schenk, 1990; Koning et al., 2005).

The observation that sample ab2-45.2-djk contains relatively diverse and abundant sanidine grains consistent with derivation from the San Juan volcanic field (Fig. 16) suggests input of sand into the study area around 14.8 Ma by the Tamaya paleodrainage, which was likely eroding into the early Oligocene sand and gravelly sand cap sourced from the San Juan volcanic field on the Colorado Plateau north of latitude 36°N (Fig. 19), as interpreted by Cather et al. (2008) and Koning et al. (2021a). The presence of sanidines with ages consistent with the Mogollon-Datil volcanic field in the ab2-45.2-djk sample could reflect input of sand by more southerly piedmont drainages (see below). Alternatively, the Mogollon-Datil grains could have been transported northward into the Tamaya paleodrainage by northeastward prevailing winds, effectively mixing these grains with the northerly sourced San Juan sanidine grains (Fig. 19).

### *Synthesis of Geologic History and Depositional Controls*

This section describes the paleogeographic and geologic history of the Ceja del Rio Puerco from 21 through 9 Ma. The narrative synthesizes the aforementioned interpretations of depositional environments, provenance, and age data (fossil and radiometric). The role of allogenic drivers (i.e., paleoclimate and tectonics) versus autogenic drivers in sedimentation during this time is also explored.

**Early Phase (21–17.5 Ma): Dune Field Transition to Fluvial-Dominated Sedimentation**

An eolian dune field occupied most of the study area between 21 and 19 Ma, as recorded by the Piedra Parada Member of the Zia Formation, followed by a gradual change to fluvial deposition during 19–17.5 Ma. The source of the eolian sand for the Piedra Parada Member was likely to the west or southwest (Fig. 18A), based on the presence of pebble-bearing, fluvial sandstones in the Piedra Parada Member about 10 km southwest of the study area (Fig. 1, location A) and the eastward dip of eolian foresets (Gawne, 1981b). Chamisa Mesa deposition represents fluvial deposition mixed with eolian deposition (with eolian processes being most common in the lower half), which is interpreted to have occurred on the transitional zone between the distal piedmont and basin floor (Fig. 18B). Because $\delta^{13}C$ and $\delta^{18}O$ isotope values remained relatively constant between 20 and 17.5 Ma (Rugenstein et al., 2026), we infer that the environmental shift was driven primarily by reorganization that could be shifting or major avulsion of the western fluvial system supplying eolian sand (autogenic), rather than by climate change. This early phase of deposition culminated with deposition of a clayey unit (Cañada Pilares Member) on a broad floodplain or small playa lake. The coincidence of the clayey sediment with the hanging wall of the Moquino fault is noteworthy, and active subsidence of this fault may have controlled the location of this unit. The presence of a local angular unconformity 1.4 km west of the Benavidez diatreme supports syndepositional movement along the Moquino fault. However, there is no evidence of facies changes or thickening changes across the Pilares fault, so movement along that fault appears to have largely postdated 18.1–17.5 Ma.

**Middle Phase (15–13 Ma): Fluvial-Dominated, Sandy Sedimentation**

An alternating distal-piedmont and basin-floor environment prevailed in the study area during deposition of Cerro Conejo Formation strata that overlie its lower unconformity. The basin floor transitioned northward to the Tamaya megafan sourced from the southeastern Colorado Plateau (Fig. 19).

A lake (or playa lake) occupied this area briefly during 14.1–14.0 Ma (preferred age), as indicated by the green marker bed in the upper tongue of unit 2 of the mixed-provenance unit (Ncm2). Like the earlier Cañada Pilares playa lake or floodplain, this clayey deposit coincides with the hanging wall of the Moquino fault and may be related to accentuated tectonic subsidence along this fault. Such subsidence might be expected to produce a wedge of coarse sediment (probably medium to very coarse sand) shed from the fault footwall that might underlie the greenish clay near the fault, but such a coarse wedge was not obvious near the stratigraphic sections. Future detailed study of the green marker clay closer to the Moquino fault, west of the Benavidez maar, may reveal the presence of such a coarse wedge. A relatively wet paleoclimate can be inferred to produce a shallow lake responsible for the fine-grained deposition and gleyed colors of the green marker bed, but an anomaly in the $\delta^{13}C$ and $\delta^{18}O$ concentrations is not indicated in the data (Rugenstein et al., 2026).

The ~17–15 Ma Cerro Conejo intraformational unconformity is significant and reflects a period of minimal sedimentation and perhaps erosion. The extensive nature of this unconformity and its long time span (2 Myr) strongly suggests climatic and/or tectonic drivers. As a working hypothesis, the presence of the unconformity may be related to high throw rates on faults to the east (e.g., Sand Hill, San Ysidro, and Zia faults) and relatively low sedimentation rates in the study area. Tectonic tilt rates were relatively high during 17–15 Ma (Fig. 17) and probably reflective of overall high rates of tectonic activity that may have accompanied this conjectured increase in throw rates along these eastern faults. If the high stratal accumulation rate of the Cañada Pilares Member was an anomaly, then the low stratal accumulation rates interpreted for 19–18 Ma Zia Formation strata (Fig. 17) continued to 17–15 Ma. Likewise, the relatively high modeled soil respiration rates and inferred high plant productivity interpreted for 19–17 Ma may have extended to (and perhaps increased during) the 17–15 Ma period of interest (Spaur et al., 2025; Rugenstein et al., 2026, fig. 7); this "greener" landscape may have been accompanied by lower erosion and sediment delivery rates. Comparison to another well-studied rift basin, the Española Basin, also indicates relatively low stratal accumulation rates between 17 and 16 Ma (Spaur et al., 2025; Koning et al., 2026d). According to paleoenvironmental interpretations in the Española Basin (Williamson, 2025), the landscape there was a mix of open habitat and closed canopy, probably leaning more toward open landscapes between 16.3 and 15.3 Ma. Notable faunal turnover occurred at 15.3 Ma, accompanying a paleoecologic change to an increased proportion of woodlands. Extending these interpretations to the study area, we speculate that the earlier open habitat, perhaps due to abundant shrubs, may have created a more stable landscape, but the 15.3 Ma ecologic change perhaps resulted in increased sedimentation.

**Late Phase (13–9 Ma): Piedmont Progradation and Change to Gravelly Deposition**

Between 13.0 and 10 Ma, the western piedmont toe shifted eastward by >4 km and then shifted slightly eastward again during early Navajo Draw Member deposition (Figs. 18C and 18D). This was immediately preceded (13.6–13.0 Ma) by southward progradation and possible general coarsening of the paleofan on the southeastern (downstream) end of the Tamaya paleodrainage, resulting in the sand-dominated deposition of Ncm4. During this time, tectonic tilt rates and stratal accumulation rates were decreasing (Fig. 17). However, $\delta^{18}O$ values clearly increased (Rugenstein et al., 2026), suggesting progressively more moisture delivery by summer precipitation events as the region transitioned to an overall drier climate after 13 Ma (Spaur et al., 2025). This increase in summer precipitation may be associated with more frequent, high-intensity convective storms, as seen today and inferred for the Holocene (Osborn and Reynolds, 1963; Drissel and Osborn, 1968; Etheredge et al., 2004).

Given that tectonic tilt rates decreased during 13–10 Ma but summer moisture increased, we invoke paleoclimatic changes as the primary driver of this progradation. During post-13 Ma drying, overall sediment flux rates may have lessened, which,

combined with a transition to a tectonically driven, sediment-bypass regime (see next paragraph), could account for the decrease in stratal accumulation rates after 13 Ma (Fig. 17, Appendices 4 and 5). Perhaps the increase of high-intensity, convective summer storms disproportionately increased erosion and sedimentation in the presumably smaller drainages associated with the western piedmont, compared to the larger Tamaya paleofan, and this imbalance would have driven progradation of the piedmont slope. As a relevant analogy, a comparative study in Arizona of drainage size, discharge, and mode of precipitation indicated that smaller drainages are impacted relatively more (in terms of discharge and related channel attributes) by localized convective summer storms and larger drainages are more affected by winter precipitation (Etheredge, 2004).

Another possible explanation for the 13–10 Ma progradation that could have occurred concomitant with the previous explanation is a conjectured decrease of vertical displacement rate on the Moquino fault and a relative increase on faults east of the study area, such as the Sand Hill, San Ysidro, and Zia faults (Fig. 1). This hypothetical increase in vertical displacement rates might be due to fault lengthening over time due to progressive integration of fault segments (Anders and Schlische, 1994; Dawers and Anders, 1995; Mansfield and Cartwright, 2001). This would focus deposition to the hanging walls of those faults. An eastward shift in fault activity would also promote sediment bypass in the study area, decrease stratal accumulation rates, and facilitate progradation of the western piedmont.

At around 10 Ma, gravelly beds became much more common in the Santa Fe Group along the Ceja del Rio Puerco, in both the Navajo Draw and Benavidez Members of the Arroyo Ojito Formation. This change occurred during a period of relatively low tilt rates and after the 13–10 Ma progradation of the western piedmont. Presently, no local $\delta^{13}C$ or $\delta^{18}O$ data exist to evaluate possible paleoclimate changes for 12–8 Ma.

Three possible factors can be invoked to explain the increase in gravel at ~10 Ma in the Benavidez and Navajo Draw Members of the Arroyo Ojito Formation. First, the 13–10 Ma progradation and shift to bypass conditions, driven by paleoclimate and/or tectonic drivers, could have promoted incision across much of the medial to proximal piedmont. The resulting channels could have more effectively delivered gravel to the distal fans and adjoining basin floor. This explanation is particularly fitting for the Benavidez Member piedmont, but an analogous phenomenon could possibly have occurred in the presumably larger Navajo Draw fluvial system. Broad uplift along the Jemez lineament, concurrent with initiation of major volcanism in the Jemez Mountains (Kelley et al., 2013a), could also have contributed to this incision.

Second, emergence of the Nacimiento Mountains, either due to progressive landscape exhumation or magmatic uplift along this section of the Jemez lineament in conjunction with major Jemez Mountain volcanism (Kelley et al., 2013a), could have contributed to the ~10 Ma increase in gravel flux in two ways: (1) it could have redirected the Tamaya paleodrainage southward and concentrated what was once multiple channels into fewer (perhaps just one) channel, thereby increasing discharge and competency, and (2) the emergence of the Nacimiento Mountains would have created steeper slopes and facilitated erosion of gravel and other sediment from that source area. A cap of weakly consolidated gravel, called the Ritito Conglomerate, would have been a ready source of Pedernal chert, quartzite, granite, and quartz (Kelley et al., 2013b).

A third explanation, especially relevant for Navajo Draw Member deposits, involves a change in exposed lithology in the upper drainage area that, in turn, changed permeability and infiltration rates of surface precipitation and runoff. As previously discussed, the Zia and Cerro Conejo Formations are interpreted to reflect erosion of a generally weakly lithified and permeable cap of Oligocene-aged gravelly sand on the southeastern Colorado Plateau. In contrast, previous studies interpreted the Navajo Draw Member sediment as reflecting reworking of Cretaceous units by a south-southeast fluvial system (Connell et al., 1999; Brandes, 2002; Connell, 2004), which we envision as a younger version of the Tamaya paleodrainage. The overall lower permeability of the Cretaceous strata (i.e., cemented sandstones, abundant mudstones) would contrast with the inferred higher permeabilities in the Oligocene sand and gravelly sand cap on the adjoining Colorado Plateau. Once the Tamaya paleodrainage eroded through this permeable, capping sediment and encountered Upper Cretaceous strata, less infiltration and more surface runoff might be expected. This would increase discharges during storm events and enhance transport of gravel from the remaining patches of Oligocene gravelly sediment.

## Conclusions

New geochronological, sedimentologic, and paleoflow/provenance data were synthesized with preexisting biostratigraphic and magnetostratigraphic data to refine depositional ages and paleoenvironmental interpretations of the lower–middle Santa Fe Group along the Ceja del Rio Puerco. The ages for the Chamisa Mesa and Cañada Pilares Members are revised to 19.0–18.1 Ma and 18.1–17.5 Ma, respectively. We retain the original placement by Gawne (1981a, 1981b) of the upper contact of the Cañada Pilares Member at the top of a 30- to 38-m-thick clay-rich interval. A cryptic intraformational unconformity (or condensed section) spanning ~2 Myr separates 17.5–17.0 Ma strata in the basal ~30 m of the Cerro Conejo Formation from 15–9 Ma strata in the upper part of the unit. Three stratigraphic units are recognized within the Cerro Conejo Formation: a western-piedmont unit that sloped east to southeast; a northern-fluvial unit deposited on a broad, south-sloping megafan (distributive fluvial system) by the Tamaya paleodrainage (new informal name); and a mixed-provenance unit that reflects mixing and interfingering between these other two units. Tectonic tilt rates decreased after ~13.5 Ma. Stratal accumulation rates (not decompacted) were low at 19.0–18.1 Ma, moderate at 18.1–17.5 Ma, spiked at 14.8–14.0 Ma, and decreased after 14 Ma. We propose that tectonic subsidence along the Moquino fault possibly promoted the occurrence of two short-lived lakes or playas at 18.1–17.5 Ma and ~14.1–14.0 Ma. Between 13 and 10 Ma, a paleoclimatic shift from wintertime to increasing summer precipitation and/or a posited eastward shift of rift fault activity is interpreted to have driven >4 km of eastward progradation of the western piedmont.

## Acknowledgments

We thank Santa Ana Pueblo and the Benavidez family for access to their lands, and Thu Bui, Gabriela Sanchez Ortiz, and Xueyao Cheng for assistance in the field. Jack Oviatt inspected three samples of clay from the Cañada Pilares Member for ostracods. We also thank Steve Cather and Brian Hampton for reviewing this manuscript. This study was partially funded by National Science Foundation grant EAR-2202916 to Rugenstein. This project is a derivative of earlier mapping and fieldwork funded by the STATEMAP component of the National Cooperative Geologic Mapping Program.

# References


Albright, L.B., Woodburne, M.O., Fremd, T.J., Swisher, C.C., III, MacFadden, B.J., and Scott, G.R., 2008, Revised chronostratigraphy and biostratigraphy of the John Day Formation (Turtle Cove and Kimberly Members), Oregon, with implications for updated calibration of the Arikareean North American Land Mammal Age: Journal of Geology, v. 116, no. 3, p. 211–237. https://doi.org/10.1086/587650

Anders, M.H., and Schlische, R.W., 1994, Overlapping faults, intrabasin highs, and growth of normal faults: Journal of Geology, v. 102, no. 2, p. 165–180. https://doi.org/10.1086/629661

Beckner, J.R., and Mozley, P.S., 1998, Origin and spatial distribution of early vadose and phreatic calcite cements in the Zia Formation, Albuquerque Basin, New Mexico, USA, *in* Morad, S., ed., Carbonate Cementation in Sandstones—Distribution patterns and geochemical evolution: Oxford, International Association of Sedimentologists and Blackwell Science, p. 27–52. https://doi.org/10.1002/9781444304893.ch2

Brandes, N.N., 2002, Lithostratigraphy and petrography of upper Santa Fe Group deposits in the northern Albuquerque Basin, New Mexico [unpublished MS thesis]: Socorro, New Mexico Institute of Mining and Technology, 208 p.

Bristow, C., and Mountney, N.P., 2013, Aeolian stratigraphy, *in* Shroder, J.F., ed., Treatise on Geomorphology, v. 11: San Diego, CA, Academic Press, p. 246–268. https://doi.org/10.1016/B978-0-12-374739-6.00306-7

Bryan, K., and McCann, F.T., 1937, The Ceja del Rio Puerco—A border feature of the Basin and Range province in New Mexico—I. Stratigraphy and structure: Journal of Geology, v. 45, no. 8, p. 801–828. https://doi.org/10.1086/624608

Bryan, K., and McCann, F.T., 1938, The Ceja del Rio Puerco—A border feature of the Basin and Range province in New Mexico—II. Geomorphology: Journal of Geology, v. 46, no. 1, p. 1–16. https://doi.org/10.1086/624618

Cather, S.M., 2004, Laramide orogeny in central and northern New Mexico and southern Colorado, *in* Mack, G.H., and Giles, K.A., eds., The Geology of New Mexico—A geologic history: New Mexico Geological Society Special Publication 11, p. 203–248. https://doi.org/10.56577/SP-11

Cather, S.M., Connell, S.D., Heynekamp, M.R., and Goodwin, L.B., 1997, Geology of the Arroyo de las Calabacillas (Sky Village SE) 7.5-minute quadrangle, Sandoval County, New Mexico: New Mexico Bureau of Mines and Mineral Resources Open-File Geologic Map 9, scale 1:24,000. https://doi.org/10.58799/of-gm-9

Cather, S.M., Connell, S.D., Chamberlin, R.M., McIntosh, W.C., Jones, G.E., Potochnik, A.R., Lucas, S.G., and Johnson, P.S., 2008, The Chuska erg—Paleogeomorphic and paleoclimatic implications of an Oligocene sand sea on the Colorado Plateau: GSA Bulletin, v. 120, no. 1–2, p. 13–33. https://doi.org/10.1130/B26081.1

Cather, S.M., Chapin, C.E., and Kelley, S.A., 2012, Diachronous episodes of Cenozoic erosion in southwestern North America and their relationship to surface uplift, paleoclimate, paleodrainage, and paleoaltimetry: Geosphere, v. 8, no. 6, p. 1177–1206. https://doi.org/10.1130/GES00801.1

Cenozoic $CO_2$ Proxy Integration Project Consortium, 2023, Toward a Cenozoic history of atmospheric $CO_2$: Science, v. 382, no. 6675, eadi5177. https://doi.org/10.1126/science.adi5177

Cikoski, C.T., Koning, D.J., and Connell, S.D., 2012, Geologic map of the La Mesita Negra 7.5-minute quadrangle, Bernalillo County, New Mexico: New Mexico Bureau of Geology and Mineral Resources Open-File Geologic Map 223, scale 1:24,000. https://doi.org/10.58799/of-gm-223

Compton, R.R., and Compton, J.S., 1985, Geology in the Field: New York, Wiley, 416 p.

Connell, S.D., 2004, Geology of the Albuquerque Basin and tectonic development of the Rio Grande rift in north-central New Mexico, *in* Mack, G.H., and Giles, K.A., eds., The Geology of New Mexico—A geologic history: New Mexico Geological Society Special Publication 11, p. 359–388. https://doi.org/10.56577/SP-11

Connell, S.D., 2008a, Geologic map of the Albuquerque–Rio Rancho metropolitan area and vicinity, Bernalillo and Sandoval Counties, New Mexico: New Mexico Bureau of Geology and Mineral Resources Geologic Map 78, scale 1:50,000, 2 sheets. https://doi.org/10.58799/gm-78

Connell, S.D., 2008b, Refinements to the stratigraphic nomenclature of the Santa Fe Group, northwestern Albuquerque Basin, New Mexico: New Mexico Geology, v. 30, no. 1, p. 14–35. https://doi.org/10.58799/nmg-v30n1.14

Connell, S.D., Koning, D.J., and Cather, S.M., 1999, Revisions to the stratigraphic nomenclature of the Santa Fe Group, northwestern Albuquerque Basin, New Mexico, *in* Pazzaglia, F.J., and Lucas, S.G., eds., Albuquerque Geology: New Mexico Geological Society Fall Field Conference Guidebook 50, p. 337–353. https://doi.org/10.56577/ffc-50.337

Connell, S.D., Koning, D.J., Kelley, S.A., and Brandes, N.N., 2007, Oligocene and early Miocene sedimentation in the southwestern Jemez Mountains and northwestern Albuquerque Basin, New Mexico, *in* Kues, B.S., Kelley, S.A., and Lueth, V.W., eds., Geology of the Jemez Region II: New Mexico Geological Society Fall Field Conference Guidebook 58, p. 195–208. https://doi.org/10.56577/FFC-58.195

Connell, S.D., Koning, D.J., and Jochems, A.P., 2026, Fault-stratigraphic relationships across the Sand Hill and San Ysidro fault zones, northwestern Albuquerque Basin, New Mexico—Implications for paleoseismic studies of low-slip-rate faults in semiarid settings, *in* Connell, S.D., and Koning, D.J., eds., Geology of the Albuquerque Region: New Mexico Geological Society Fall Field Conference Guidebook 76, p. 277–290. https://doi.org/10.56577/FFC-76.277

Dawers, N.H., and Anders, M.H., 1995, Displacement-length scaling and fault linkage: Journal of Structural Geology, v. 17, no. 5, p. 607–614. https://doi.org/10.1016/0191-8141(94)00091-D

Dethier, D.P., and Manley, K., 1985, Geologic map of the Chili quadrangle, Rio Arriba County, New Mexico: U.S. Geological Survey Miscellaneous Field Studies Map 1814, scale 1:24,000. https://doi.org/10.3133/mf1814

Dettman, D.L., Fang, X., Garzione, C.N., and Li, J., 2003, Uplift-driven climate change at 12 Ma—A long $\delta^{18}O$ record from the NE margin of the Tibetan plateau: Earth and Planetary Science Letters, v. 214, no. 1–2, p. 267–277. https://doi.org/10.1016/S0012-821X(03)00383-2

Drissel, J.C., and Osborn, H.B., 1968, Variability in rainfall producing runoff from a semiarid rangeland watershed, Alamogordo Creek, New Mexico: Journal of Hydrology, v. 6, no. 2, p. 194–201. https://doi.org/10.1016/0022-1694(68)90159-5

Etheredge, D., Gutzler, D.S., and Pazzaglia, F.J., 2004, Geomorphic response to seasonal variations in rainfall in the southwest United States: GSA Bulletin, v. 116, no. 5–6, p. 606–618. https://doi.org/10.1130/B22103.1

Frick, C., and Taylor, B.E., 1968, A generic review of the stenomyline camels: American Museum Novitates, no. 2353, 51 p. http://hdl.handle.net/2246/2563

Galusha, T., 1966, The Zia Sand Formation, new early to medial Miocene beds in New Mexico: American Museum Novitates, no. 2271, 12 p. http://hdl.handle.net/2246/3237

Galusha, T., and Blick, J.C., 1971, Stratigraphy of the Santa Fe Group, New Mexico: Bulletin of the American Museum of Natural History, v. 144, article 1, 127 p. http://hdl.handle.net/2246/1633

Gawne, C.E., 1981a, Sedimentology and stratigraphy of the Miocene Zia Sand of New Mexico—Summary: GSA Bulletin, v. 92, no. 12, p. 999–1007. https://doi.org/10.1130/0016-7606(1981)92%3C999:sasotm%3E2.0.co;2

Gawne, C.E., 1981b, Sedimentology and stratigraphy of the Miocene Zia Sand of New Mexico: GSA Bulletin, v. 92, no. 12, part II, p. 2484–2552. https://doi.org/10.1130/GSAB-P2-92-2484

Grauch, V.J.S., and Connell, S.D., 2013, New perspectives on the geometry of the Albuquerque Basin, Rio Grande rift, New Mexico—Insights from geophysical models of rift-fill thickness, *in* Hudson, M.R., and Grauch, V.J.S., eds., New perspectives on Rio Grande rift basins—From tectonics to groundwater: Geological Society of America Special Paper 494, p. 427–462. https://doi.org/10.1130/2013.2494(16)

Hartley, A.J., Weissmann, G.S., Nichols, G.J., and Warwick, G.L., 2010, Large distributive fluvial systems—Characteristics, distribution, and controls on development: Journal of Sedimentary Research, v. 80, no. 2, p. 167–183. https://doi.org/10.2110/jsr.2010.016

Kelley, V.C., 1977, Geology of Albuquerque Basin, New Mexico: New Mexico Bureau of Mines and Mineral Resources Memoir 33, 60 p. https://doi.org/10.58799/M-33

Kelley, S.A., McIntosh, W.C., Goff, F., Kempter, K.A., Wolff, J.A., Esser, R., Braschayko, S., Love, D., and Gardner, J.N., 2013a, Spatial and temporal trends in pre-caldera Jemez Mountains volcanic and fault activity: Geosphere, v. 9, no. 3, p. 614–646. https://doi.org/10.1130/GES00897.1

Kelley, S.A., Kempter, K.A., McIntosh, W.C., Maldonado, F., Smith, G.A., Connell, S.D., Koning, D.J., and Whiteis, J., 2013b, Syndepositional deformation and provenance of Oligocene to lower Miocene sedimentary rocks along the western margin of the Rio Grande rift, Jemez Mountains, New Mexico, *in* Hudson, M., and Grauch, V.J.S., eds., New perspectives on Rio Grande rift basins—From tectonics to groundwater: Geological Society of America Special Paper 494, p. 101–123, https://doi.org/10.1130/2013.2494(05)

Koning, D.J., 2002, Geologic map of the Española 7.5-minute quadrangle, Rio Arriba and Santa Fe Counties, New Mexico: New Mexico Bureau of Geology and Mineral Resources Open-File Geologic Map 54, scale 1:24,000. https://doi.org/10.58799/OF-GM-54

Koning, D.J., and Jochems, A.P., 2014, Geologic map of the Benavidez Ranch 7.5-minute quadrangle, Bernalillo and Sandoval Counties, New Mexico: New Mexico Bureau of Geology and Mineral Resources Open-File Geologic Map 234, scale 1:24,000. https://doi.org/10.58799/of-gm-234

Koning, D.J., and Personius, S.F., 2002, Geologic map of the Bernalillo NW quadrangle, Sandoval County, New Mexico: U.S. Geological Survey Miscellaneous Field Studies Map 2404, scale 1:24,000. https://doi.org/10.3133/mf2404

Koning, D.J., and Rawling, G.C., 2017, Geologic map of the San Felipe Mesa 7.5-minute quadrangle, Sandoval County, New Mexico: New Mexico Bureau of Geology and Mineral Resources Open-File Geologic Map 266, scale 1:24,000. https://doi.org/10.58799/of-gm-266

Koning, D.J., Pederson, J., Pazzaglia, F.J., and Cather, S.M., 1998, Geology of the Cerro Conejo (Sky Village NE) 7.5-minute quadrangle, Sandoval County, New Mexico: New Mexico Bureau of Mines and Mineral Resources Open-File Geologic Map 45, scale 1:24,000. https://doi.org/10.58799/of-gm-45

Koning, D.J., Skotnicki, S.J., Kelley, S.A., and Moore, J., 2005, Geologic map of the Chili 7.5-minute quadrangle, Rio Arriba County, New Mexico: New Mexico Bureau of Geology and Mineral Resources Open-File Geologic Map 103, scale 1:24,000. https://doi.org/10.58799/OF-GM-103

Koning, D.J., Grauch, V.J.S., Connell, S.D., Ferguson, J., McIntosh, W., Slate, J.L., Wan, E., and Baldridge, W.S., 2013, Structure and tectonic evolution of the eastern Española Basin, Rio Grande rift, north-central New Mexico, *in* Hudson, M., and Grauch, V.J.S., eds., New perspectives on Rio Grande rift basins—From tectonics to groundwater: Geological Society of America Special Paper 494, p. 185–219, https://doi.org/10.1130/2013.2494(08)

Koning, D.J., Jochems, A.P., Foster, R., Cox, B., Lucas, S.G., Mack, G.H., and Zeigler, K.E., 2018, Geologic map of the Cuchillo 7.5-minute quadrangle, Sierra County, New Mexico: New Mexico Bureau of Geology and Mineral Resources Open-File Geologic Map 271, scale 1:24,000. https://doi.org/10.58799/OF-GM-271

Koning, D.J., Jochems, A.P., Hobbs, K.M., Pearthree, K.S., and Love, D.W., 2020, Geologic map of the Paraje Well 7.5-minute quadrangle, Socorro County, New Mexico: New Mexico Bureau of Geology and Mineral Resources Open-File Geologic Map 286, scale 1:24,000. https://doi.org/10.58799/OF-GM-286

Koning, D.J., Heizler, M., and Jochems, A., 2021a, Clues from the Santa Fe Group for Oligocene–Miocene paleogeography of the southeastern Colorado Plateau near Grants, NM, *in* Frey, B.A., Kelley, S.A., Goff, F., Zeigler, K.E., McLemore, V.T., and Ulmer-Scholle, D.S., eds., Geology of the Mount Taylor Area: New Mexico Geological Society Fall Field Conference Guidebook 71, p. 267–280. https://doi.org/10.56577/FFC-71.267

Koning, D.J., Hobbs, K.M., Pearthree, K.S., and Love, D.W., 2021b, Geologic map of the Fort Craig 7.5-minute quadrangle, Socorro County, New Mexico: New Mexico Bureau of Geology and Mineral Resources Open-File Geologic Map 288, scale 1:24,00. https://doi.org/10.58799/OF-GM-288

Koning, D.J., Martin, L., Zimmerer, M.J., Mamer, E., Doherty, A.L.M., Sturgis, L., and Dunbar, N.W., 2026a, Investigation of hydrostratigraphic units of the Santa Fe Group aquifer in the northwestern Albuquerque Basin, New Mexico: New Mexico Bureau of Geology and Mineral Resources Open-File Report 635, 77 p. and 17 plates. https://doi.org/10.58799/OFR-635

Koning, D.J., Martin, L., and Sturgis, L., 2026b, Development of a 3D hydrostratigraphic model in the northwestern Albuquerque Basin, New Mexico—Implications for the Santa Fe Group aquifer, stratigraphy, and rift structure, *in* Connell, S.D., and Koning, D.J., eds., Geology of the Albuquerque Region: New Mexico Geological Society Fall Field Conference Guidebook 76, p. 351–359. https://doi.org/10.56577/FFC-76.351

Koning, D.J., Connell, S.D., Rugenstein, J.K., Lucas, S.G., and Rawling, G., 2026c, Second-day road log—Northwest Albuquerque Basin, Rio Rancho and Ceja del Rio Puerco, *in* Connell, S.D., and Koning, D.J., eds., Geology of the Albuquerque Region: New Mexico Geological Society Fall Field Conference Guidebook 76, p. 47–86. https://doi.org/10.56577/FFC-76.47

Koning, D.J., Spaur, S., Williamson, G., and Rugenstein, J.C., 2026d, What you can do with superb rift basin-fill exposures—Recent lithostratigraphic, paleoclimatic, biostratigraphic, and structural studies of the Española Basin, New Mexico, USA, *in* Wintsch, R.P., Drzewiecki, P.A., and Hobbs, K.M., eds., Investigating Paleoenvironments and Provenance in Sedimentary and Metasedimentary Basins—New York, New Mexico, and Connecticut: Geological Society of America Field Guide 77, p. 85–108. https://doi.org/10.1130/2026.0077(04)

Kuiper, K.F., Deino, A., Hilgen, F.J., Krijgsman, W., Renne, P.R., and Wijbrans, J.R., 2008, Synchronizing rock clocks of Earth history: Science, v. 320, no. 5875, p. 500–504. https://doi.org/10.1126/science.1154339

Lipman, P.W., and McIntosh, W.C., 2008, Eruptive and noneruptive calderas, northeastern San Juan Mountains, Colorado—Where did the ignimbrites come from?: GSA Bulletin, v. 120, no. 7–8, p. 771–795. https://doi.org/10.1130/B26330.1

Lipman, P.W., and Zimmerer, M.J., 2019, Magmato-tectonic links—Ignimbrite calderas, regional dike swarms, and transition from arc to rift in the Southern Rocky Mountains: Geosphere, v. 15, no. 6, p. 1893–1926. https://doi.org/10.1130/GES02068.1

Mahon, K.I., 1996, The New "York" regression—Application of an improved statistical method to geochemistry: International Geology Review, v. 38, no. 4, p. 293–303. https://doi.org/10.1080/00206819709465336

Maldonado, F., Budahn, J.R., Peters, L., and Unruh, D.M., 2006, Geology, geochronology, and geochemistry of basaltic flows of the Cat Hills, Cat Mesa, Wind Mesa, Cerro Verde, and Mesita Negra, central New Mexico: Canadian Journal of Earth Sciences, v. 43, no. 9, p. 1251–1268. https://doi.org/10.1139/E06-018

Mansfield, C., and Cartwright, J., 2001, Fault growth by linkage—Observations and implications from analogue models: Journal of Structural Geology, v. 23, no. 5, p. 745–763. https://doi.org/10.1016/S0191-8141(00)00134-6

McDougall, I., and Harrison, T.M., 1999, Geochronology and Thermochronology by the $^{40}Ar/^{39}Ar$ Method (2nd edition): New York, Oxford University Press, 269 p.

McIntosh, W.C., Geissman, J.W., Chapin, C.E., Kunk, M.J., and Henry, C.D., 1992, Calibration of the latest Eocene-Oligocene geomagnetic polarity time scale using $^{40}Ar/^{39}Ar$ dated ignimbrites: Geology, v. 20, no. 5, p. 459–463. https://doi.org/10.1130/0091-7613(1992)020<0459:COTLEO>2.3.CO;2

Min, K., Mundil, R., Renne, P.R., and Ludwig, K.R., 2000, A test for systematic errors in $^{40}Ar/^{39}Ar$ geochronology through comparison with U/Pb analysis of a 1.1-Ga rhyolite: Geochimica et Cosmochimica Acta, v. 64, no. 1, p. 73–98. https://doi.org/10.1016/S0016-7037(99)00204-5

Morgan, G.S., 2015, Oligocene and Miocene vertebrates from New Mexico, *in* Lucas, S.G., and Sullivan, R.M., eds., Vertebrate Paleontology in New Mexico: New Mexico Museum of Natural History and Science Bulletin 68, p. 159–231. https://nmdigital.unm.edu/digital/collection/bulletins/id/4643/rec/1

Morgan, G.S., and Williamson, T.E., 2000, Middle Miocene (late Barstovian) vertebrates from the Benavidez Ranch local fauna, Albuquerque Basin, New Mexico, *in* Lucas, S.G., ed., New Mexico's Fossil Record 2: New Mexico Museum of Natural History and Science Bulletin 16, p. 195–207. https://nmdigital.unm.edu/digital/collection/bulletins/id/985

Morgan, G.S., and Williamson, T.E., 2007, Middle Miocene (late Barstovian) mammal and bird tracks from the Benavidez Ranch local fauna, Zia Formation, Albuquerque Basin, Sandoval County, New Mexico, *in* Lucas, S.G., Spielmann, J.A., and Lockley, M.G., eds., Cenozoic Vertebrate Tracks and Traces: New Mexico Museum of Natural History and Science Bulletin 42, p. 319–330. https://nmdigital.unm.edu/digital/collection/bulletins/id/376/rec/1

Mozley, P.S., and Davis, J.M., 1996, Relationship between oriented calcite concretions and permeability correlation structure in an alluvial aquifer, Sierra Ladrones Formation, New Mexico: Journal of Sedimentary Research, v. 66, no. 1, p. 11–16. https://doi.org/10.1306/d4268293-2b26-11d7-8648000102c1865d

Nier, A.O., 1950, A redetermination of the relative abundances of the isotopes of carbon, nitrogen, oxygen, argon, and potassium: Physical Review, v. 77, no. 6, p. 789–793. https://doi.org/10.1103/PhysRev.77.789

North American Commission on Stratigraphic Nomenclature, 2005, North American stratigraphic code: AAPG Bulletin, v. 89, no. 11, p. 1547–1591. https://doi.org/10.1306/07050504129

Ogg, J., 2020, Geomagnetic polarity time scale, *in* Gradstein, F.M., Ogg, J.G., Schmitz, M.D., and Ogg, G.M., eds., Geologic Time Scale 2020, v. 1: Amsterdam, Elsevier, p. 159–192. https://doi.org/10.1016/B978-0-12-824360-2.00005-X

Osborn, H.B., and Reynolds, W.N., 1963, Convective storm patterns in the southwestern United States: Hydrological Sciences Journal, v. 8, no. 3, p. 71–83. https://doi.org/10.1080/02626666309493339

Rawling, G.C., and Koning, D.J., 2019, Geologic map of the Herrera 7.5-minute quadrangle, Sandoval and Bernalillo Counties, New Mexico: New Mexico Bureau of Geology and Mineral Resources Open-File Geologic Map 273, scale 1:24,000. https://doi.org/10.58799/OF-GM-273

Rawling, G.C., and Koning, D.J., 2020, Geologic map of the Cañoncito School 7.5-minute quadrangle, Bernalillo and Cibola Counties, New Mexico: New Mexico Bureau of Geology and Mineral Resources Open-File Geologic Map 281, scale 1:24,000. https://doi.org/10.58799/OF-GM-281

Rugenstein, J.K.C., Bernstein, R., Walsh, A., Heizler, M., and Koning, D., 2026, Authigenic carbonate and organic carbon stable-isotope constraints on paleoenvironments and climate in the Albuquerque Basin during the Neogene, *in* Connell, S.D., and Koning, D.J., eds., Geology of the Albuquerque Region: New Mexico Geological Society Fall Field Conference Guidebook 76, p. 301–318. https://doi.org/10.56577/FFC-76.301

Schenk, C.J., 1990, Eolian deposits of the Ojo Caliente Sandstone Member (Miocene) of the Tesuque Formation, Espanola Basin, New Mexico, *in* Fryberger, S.G., Krystinik, L.F., and Schenk, C.J., eds., Modern and Ancient Eolian Deposits—Petroleum exploration and production: Denver, Rocky Mountain Section, Society of Economic Paleontologists and Mineralogists, p. 18-1–18-09.

Seager, W.R., and Mack, G.H., 2003, Geology of the Caballo Mountains, New Mexico: New Mexico Bureau of Geology and Mineral Resources Memoir 49, 144 p. https://doi.org/10.58799/M-49

Smyth, D.G., 2004, Sedimentology and permeability characteristics of the Arroyo Ojito Formation (upper Santa Fe Group) adjacent to the Sand Hill fault, Albuquerque Basin, New Mexico [MS thesis]: Socorro, New Mexico Institute of Mining and Technology, 96 p. https://www.nmt.edu/academics/ees/theses/theses_1936-2014/2004t_smyth_dg.pdf

Spaur, S., Koning, D.J., Heizler, M., Aby, S., Williamson, G., Knott, J.R., Acosta, R.P., and Rugenstein, J.K.C., 2025, The hydroclimate and environmental response to middle Miocene warming in the southwestern USA–Stable isotope evidence: Paleocenography and Paleoclimatology, v. 40, no. 5, e2024PA005056. https://doi.org/10.1029/2024PA005056

Spiegel, Z., 1961, Late Cenozoic sediments of the lower Jemez River region, *in* Northrop, S.A., ed., Albuquerque Country: New Mexico Geological Society Fall Field Conference Guidebook 12, p. 132–138. https://doi.org/10.56577/ffc-12.132

Spiegel, Z., and Baldwin, B., 1963, Geology and water resources of the Santa Fe area, New Mexico: U.S. Geological Survey Water Supply Paper 1525, 258 p. https://doi.org/10.3133/wsp1525

Tedford, R.H., 1981, Mammalian biochronology of the late Cenozoic basins of New Mexico: GSA Bulletin, v. 92, no. 12, p. 1008–1022. https://doi.org/10.1130/0016-7606(1981)92<1008:MBOTLC>2.0.CO;2

Tedford, R.H., 1982, Neogene stratigraphy of the northwestern Albuquerque Basin, *in* Grambling, J.A., Wells, S.G., and Callender, J.F., eds., Albuquerque Country II: New Mexico Geological Society Fall Field Conference Guidebook 33, p. 273–278. https://doi.org/10.56577/ffc-33.273

Tedford, R.H., and Barghoorn, S., 1997, Miocene mammals of the Española and Albuquerque Basins, *in* Lucas, S.G., Estep, J.W., Williamson, T.E., and Morgan, G.S., eds., New Mexico's Fossil Record 1: New Mexico Museum of Natural History and Science Bulletin 11, p. 77–96. https://econtent.unm.edu/digital/collection/bulletins/id/1045/rec/1v

Tedford, R.H., and Barghoorn, S.F., 1999, Santa Fe Group (Neogene), Ceja del Rio Puerco, northwestern Albuquerque Basin, Sandoval County, New Mexico, *in* Pazzaglia, F.J., and Lucas, S.G., eds., Albuquerque Geology: New Mexico Geological Society Fall Field Conference Guidebook 50, p. 327–335. https://doi.org/10.56577/ffc-50.327

Tedford, R.H., Albright, L.B., III, Barnosky, A.D., Ferrusquia-Villafranca, I., Hunt, R.M., Jr., Storer, J.E., Swisher, C.C., III, Voorhies, M.R., Webb, S.D., and Whistler, D.P., 2004, Mammalian biochronology of the Arikareean through Hemphillian interval (late Oligocene through early Pliocene epochs), *in* Woodburne, M.O., ed., Late Cretaceous and Cenozoic Mammals of North America—Biostratigraphy and geochronology: New York, Columbia University Press, p. 169–231. https://doi.org/10.7312/wood13040-008

Thompson, R.A., Shroba, R.R., Menges, C.M., Schmidt, D.L., Personius, S.F., and Brandt, T.R., 2009, Geologic map of the Volcanoes quadrangle, Bernalillo and Sandoval Counties, New Mexico: U.S. Geological Survey Scientific Investigations Map 3083, scale 1:24,000. https://doi.org/10.3133/sim3083

U.S. Department of Agriculture, 2009, National Agriculture Imagery Program (NAIP), Information Sheet: https://www.fsa.usda.gov/Internet/FSA_File/naip_2009_info_final.pdf (accessed February 24, 2026).

Weissmann, G.S., Hartley, A.J., Nichols, G.J., Scuderi, L.A., Olson, M., Buehler, H., and Banteah, R., 2010, Fluvial form in modern continental sedimentary basins—Distributive fluvial systems: Geology, v. 38, no. 1, p. 39–42. https://doi.org/10.1130/G30242.1

Wheeler, H.E., 1964, Baselevel, lithosphere surface, and time-stratigraphy: GSA Bulletin, v. 75, no. 7, p. 599–610. https://doi.org/10.1130/0016-7606(1964)75[599:BLSAT]2.0.CO;2

Williams, P.L., and Cole, J.C., 2007, Geologic map of the Albuquerque 30' x 60' quadrangle, north-central New Mexico: U.S. Geological Survey Scientific Investigations Map 2946, 31 p., scale 1:100,000. https://doi.org/10.3133/sim2946

Williamson, G.R., 2025, Late Hemingfordian–Barstovian mammalian biostratigraphy of the Tesuque Formation (Middle Miocene), Española Basin, north-central New Mexico [PhD dissertation]: Lubbock, Texas Tech University, 150 p.

Wright, H.E., Jr., 1946, Tertiary and Quaternary geology of the lower Rio Puerco area, New Mexico: GSA Bulletin, v. 57, no. 5, p. 383–456. https://doi.org/10.1130/0016-7606(1946)57[383:taqgot]2.0.co;2

## Appendices

Appendix 1. Information and detailed descriptions for stratigraphic sections.

Appendix 2. Southern Boulevard stratigraphic section (11x17 format) showing individual stratigraphic section units. Described and measured by Daniel Koning and Jeremy Rugenstein from 0 to 88 m. The upper part of the section is from Tedford and Barghoorn (1999).

Appendix 3. Orientation point data. Sheet A is for paleoflow measurements, Sheet B is for stratal dips between the Moquino and Pilares faults, and Sheet C is for stratal dips between the Pilares and Sand Hill faults. Locations given in UTM coordinates (NAD 83, zone 13), and north is 0°. Tilt rates are given in Sheet D.

Appendix 4. Data used to calculate stratal accumulation rates (not adjusted for compaction).

Appendix 5. Stratigraphic height versus age model from the middle Chamisa Mesa Member (Zia Formation) through the Cerro Conejo Formation.

Appendices are available for download at https://geoinfo.nmt.edu/repository/index.cfml?rid=20260001.